SUBMITTED BY:

Ken Pennock, Forecasting and Research Business Manager
KPennock@awstruepower.com
Ph: 518-213-0044 ext. 1075
Fax: 518-213-0045

AWS Truepower™
Where science delivers performance.

TABLE OF CONTENTS

LIST OF FIGURES

LIST OF TABLES

1. INTRODUCTION

In May 2011, AWS Truepower (AWST), in partnership with General Electric (GE), was engaged by the PJM Interconnection (PJM) to carry out the PJM Renewable Integration Study (PRIS). AWST's role in this study was to provide wind and solar power generation profiles and power forecasts within the PJM interconnection region as inputs to grid simulations to be carried out by GE. GE required a set of data that would capture in a realistic fashion both the temporal and spatial variability of the wind and solar resource and associated power generation of hypothetical and existing renewable energy power plants. These data were to be based on high-resolution simulations of the historical climate performed by a mesoscale numerical weather prediction (NWP) model covering the period 2004 to 2006.

AWST performed this work over a period of four months from June 2011 to September 2011. The map in Figure 1 shows the PRIS region, with the PJM Renewable Resource Boundary shown in red and the PJM Service Territory shown in black. The PJM Renewable Resource Boudnary includes all land area in the PJM Service Territory plus land that falls within 30 miles of a PJM facility equal or greater to 345 kV.
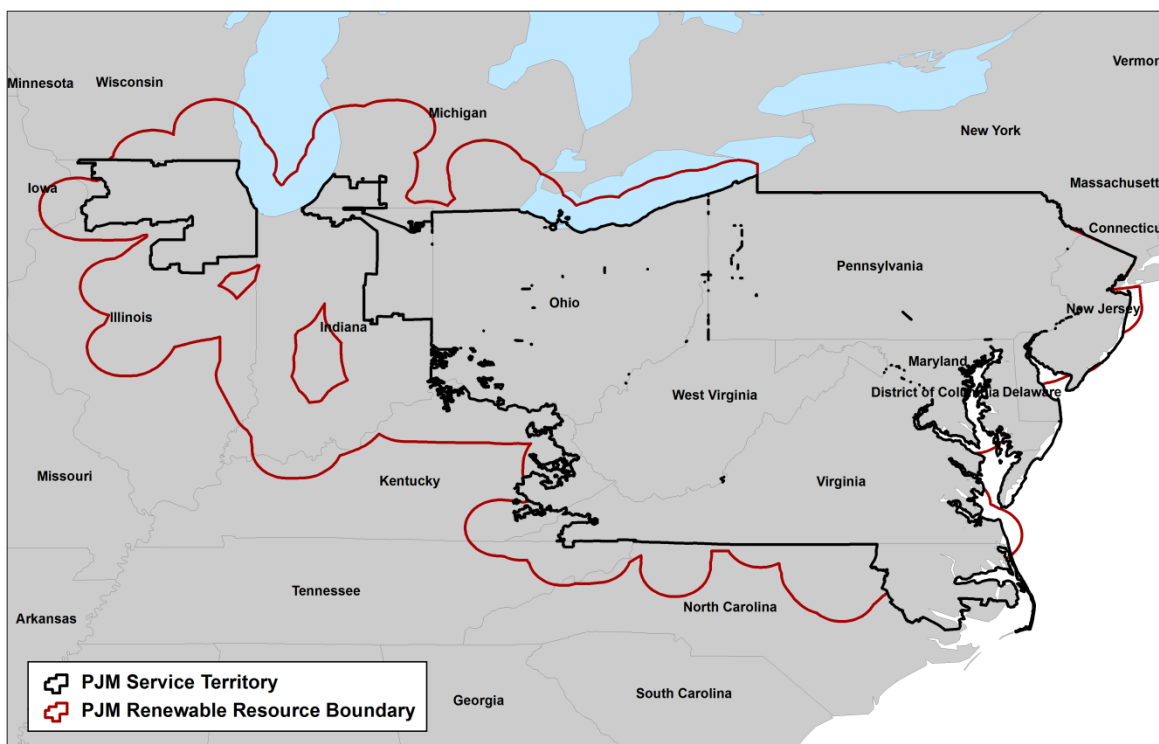
Figure 1. PJM Renewable Resource Boundary and Service Territory.

The work was divided into the following technical tasks:

- Obtain archived NWP modeled data from the Eastern Wind and Transmission Study[1] (EWITS) previously performed by AWST

---

[1] M. Brower, "Development of eastern regional wind resource and wind plant output datasets," AWS Truepower, LLC, Albany, NY, Tech. Rep. SR-550-46764. Dec. 2009. http://www.nrel.gov/wind/systemsintegration/ewits.html

- Work with PJM and stakeholders to identify likely renewable energy power plants within the PJM interconnect region

- Generate wind power output time series for onshore and offshore EWITS sites

- Generate solar power output time series for commercial, residential, and utility scale sites

- Simulate four-hour, six-hour, and next-day wind and solar power forecasts

- Compile results and report on findings

Several assumptions have been made in order to facilitate the delivery of the requested datasets. These assumptions were proposed by AWST, presented to project stakeholders, and then applied based on GE and PJM's recommendations. This document presents AWST's final technical report on the methods used, the results achieved, and a validation of the datasets.

2. MESOSCALE MODELING

The EWITS dataset was generated with the Mesoscale Atmospheric Simulation System (MASS), a proprietary model developed by AWST partner MESO, Inc[2]. MASS is a non-hydrostatic weather model which has been customized for near-surface wind and irradiance prediction. MASS simulates the fundamental physics of the atmosphere including conservation of mass, momentum, and energy as well as the moisture phases using a variety of online, global, geophysical and meteorological databases. The main meteorological inputs are reanalysis data, radiosonde data, and land surface measurements. The reanalysis database – the most important – is a gridded historical data set produced by the U.S. National Centers for Environmental Prediction and National Center for Atmospheric Research (NCEP/NCAR Reanalysis; NNGR). The data provide a snapshot of atmospheric conditions around the world at all levels of the atmosphere in intervals of six hours. Along with rawinsonde and surface data, the reanalysis data establish the initial and lateral boundary conditions for the MASS runs. The MASS model itself determines the evolution of atmospheric conditions within the region based on the interactions among different elements in the atmosphere and between the atmosphere and the surface.

The reanalysis data are on a relatively coarse grid (about 210-km spacing). To avoid generating noise at the boundaries that can result from large jumps in grid cell size, mesoscale models such as MASS are typically run using nested grids of successfully finer mesh size until the desired grid scale is reached. In this configuration, the outer grid provides initial guess fields and updated lateral boundary conditions for each subsequent nest of an inner grid. For this study, a nested grid scheme with horizontal resolutions of 30 km, 8 km, and 2 km was used (Figure 2). The runs used for the PRIS cover the eastern United States for the period 1 January 2004 to 1 January 2007. Table 1 summarizes the model configuration used in this study.

---

[2] Manobianco, J., J. W. Zack, and G.E. Taylor, 1996: Workstation-based real-time mesoscale modeling designed for weather support to operations at the Kennedy Space Center and Cape Canaveral Air Station. Bull. Amer. Meteor. Soc., 77, 653-672. Available online at http://science.ksc.nasa.gov/amu/journals/bams-1996.pdf.
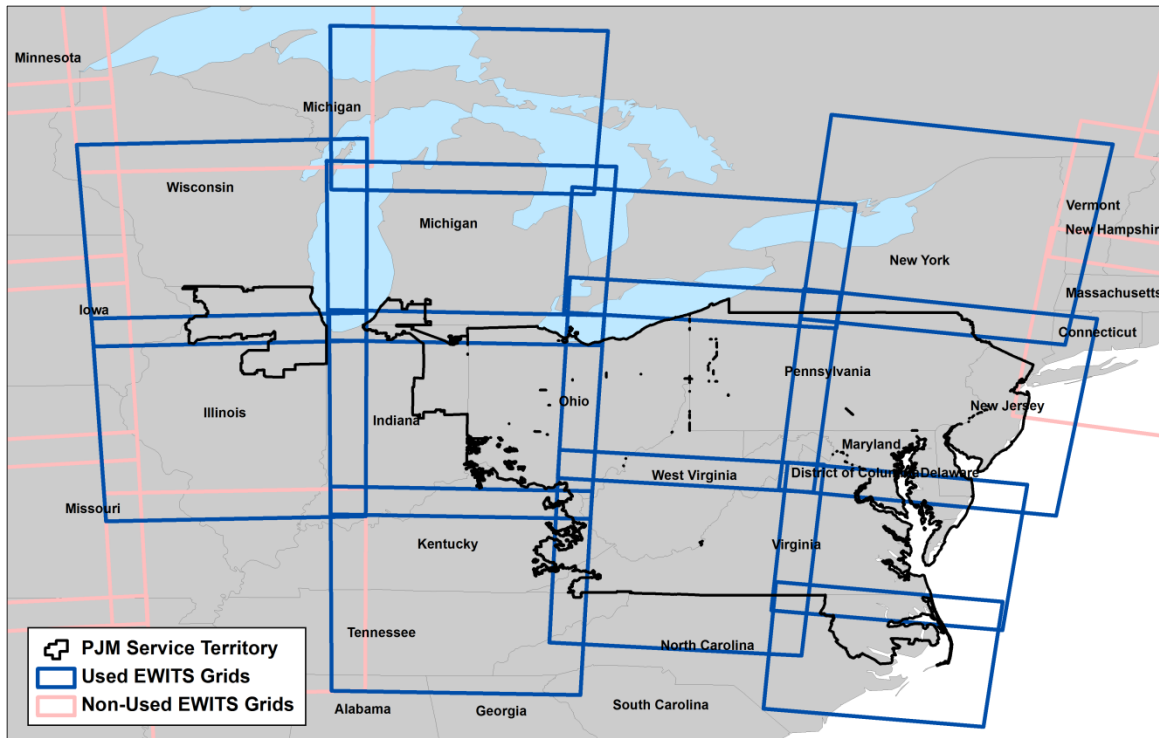
Figure 2. MASS 2-km grid configuration for EWITS, highlighting grids used for PRIS.

Table 1. Model configuration for MASS runs.

Model	MASS v. 6.8
Initialization data source	NNGR
Data to be assimilated in the course of simulations (30 km and 8 km grids only)	Rawinsonde, surface observations (temperature, dew point, wind direction and speed, pressure)
Sea-surface temperatures	MODIS (Moderate Resolution Imaging Spectroradiometer)
High-resolution terrain and land cover (2 km grid only)	US Geological Survey National Elevation Dataset and Land-Use Land-Cover Dataset, both 30 m grid spacing
Cumulus scheme (30 km and 8 km grids only)	Kain-Fritsch
Spin-up	12 hours before start of valid run
Length of run	15-16 day series (e.g., Jan 1-15, Jan 16-31)
Frequency of data sampling	Every 10 min.
Data to be stored	U, V, temperature, pressure, TKE at five heights; surface temperature and pressure, specific humidity, incoming long-wave and short-wave radiation, precipitation

3. SITE SELECTION

AWST worked with PJM and stakeholders to identify likely sites to be used for potential renewable energy projects. The sites have been selected based on their respective resource and each state's renewable energy requirement. AWST was initially tasked to propose sites that would exceed the aggregate PJM-state renewable portfolio standard (RPS) requirement of 14% renewable energy by 2026, denoted the baseline case. In support of additional scenarios proposed by the GE team, AWST was later tasked with selecting enough sites to fulfill a 30% renewable energy scenario (76.86 GW wind, 74 GW solar). This was proposed to be met with a mix of onshore and offshore wind sites as well as a mix of solar centralized and distributed generation facilities. The onshore and offshore wind sites were selected from those developed for the EWITS. For solar, the aim was to find sites containing a mix of centralized (utility-scale sites of 10–100 MW) and distributed generation. Distributed generation plants were to be made up of a mix of commercial-scale (250–1000 kW) and residential-scale (1–10 kW) locations. The following sections describe the methodology for selecting sites and the total amount of energy that they are estimated to generate. It was eventually decided that AWST would create 70% of the solar capacity from centralized sites and 70% from distributed sites to afford GE the flexibility of a range of combinations for their scenarios.

3.1. WIND

The EWITS onshore and offshore wind sites were used as the basis for the PRIS. Each theoretical "site" was defined for the EWITS as a grouping of wind turbines that represent a potential wind power plant. The size of each site is dependent on the available wind resource and its potential to be built, resulting in a large range of onshore site capacities. The sites were selected based on a seamless map of predicted mean wind speeds at 80 m height within the PJM Renewable Resource Boundary. The seamless map has a horizontal spatial resolution of 200 m, which is sufficiently fine to reflect the influence of most terrain features and to identify specific locations for wind projects. The map was adjusted during the EWITS using publicly available wind data.

A majority of the EWITS sites within the PJM Renewable Resource Boundary were used, with the exception of those that have been excluded based on additional criteria, as described below. Additional sites outside of the PJM Service Territory but within the PJM Renewable Resource Boundary were included in all energy totals in order to meet the superset requirements for wind capacity. All wind power plants in the PJM interconnection queue were modeled at the nearest EWITS site location with the actual proposed plant capacity.

The following areas were excluded from development during the site selection process:

Onshore

- Open water
- 200-m buffer of developed low intensity
- 500-m buffer of developed medium intensity
- 500-m buffer of developed high intensity
- Woody wetlands
- Emergent herbaceous wetland
- Parks
- Parks detailed
- Federal lands (non-public)

- 10,000-ft buffer of small airports (all hub sizes)
- 20,000-ft buffer of large airports (hub sizes; medium and large)
- Slopes greater than 20%
- Areas outside the study region

Offshore

- Areas within 5 miles of land
- Ocean depth greater than 30m
- Shipping lanes
- Anchorage areas
- Beacons/buoys
- Cables/pipes
- Dumping grounds
- Military practice areas
- Obstruction/wreckage
- Offshore platforms

A total of 302 onshore and 4269 offshore sites totaling 108.12 and 85.38 GW of capacity, respectively, were selected from the EWITS sites. The selected sites' total projected wind power plant capacity amounts to 193.50 GW. Selected wind sites are summarized by state in Table 2. A map of all onshore and offshore wind sites is shown in Figure 3. Additionally, all planned wind power facilities with signed agreements in the PJM queue were included with the projected plants.

Table 2. Wind projected and planned queue site capacities by state.

State	Onshore		Offshore		Queue		Total	
	Count	GW	Count	GW	Count	GW	Count	GW
DE	7	1.02	111	2.22	1	0.45	119	3.69
IA	1	0.30	33	0.66	0	0.00	34	0.96
IL	63	35.45	3	0.06	71	12.58	137	48.10
IN	58	29.78	-	-	34	7.31	92	37.09
KY	6	1.49	-	-	1	0.06	7	1.55
MD	9	1.11	354	7.08	8	0.72	371	8.91
MI	14	5.96	18	0.36	6	1.17	38	7.49
NJ	8	1.33	657	13.14	4	0.39	669	14.86
NC	4	0.48	1385	27.70	0	0.00	1389	28.18
OH	34	17.45	606	12.12	42	7.41	682	36.97
PA	56	6.99	123	2.46	67	8.92	246	18.36
TN	1	0.10	-	-	0	0.00	1	0.10
VA	16	2.10	979	19.58	6	0.48	1001	22.16
WI	7	2.20	-	-	0	0.00	7	2.20
WV	18	2.38	-	-	14	1.50	32	3.87
Total	**302**	**108.12**	**4269**	**85.38**	**254**	**40.99**	**4825**	**234.49**

AWS Truepower™
Where science delivers performance.
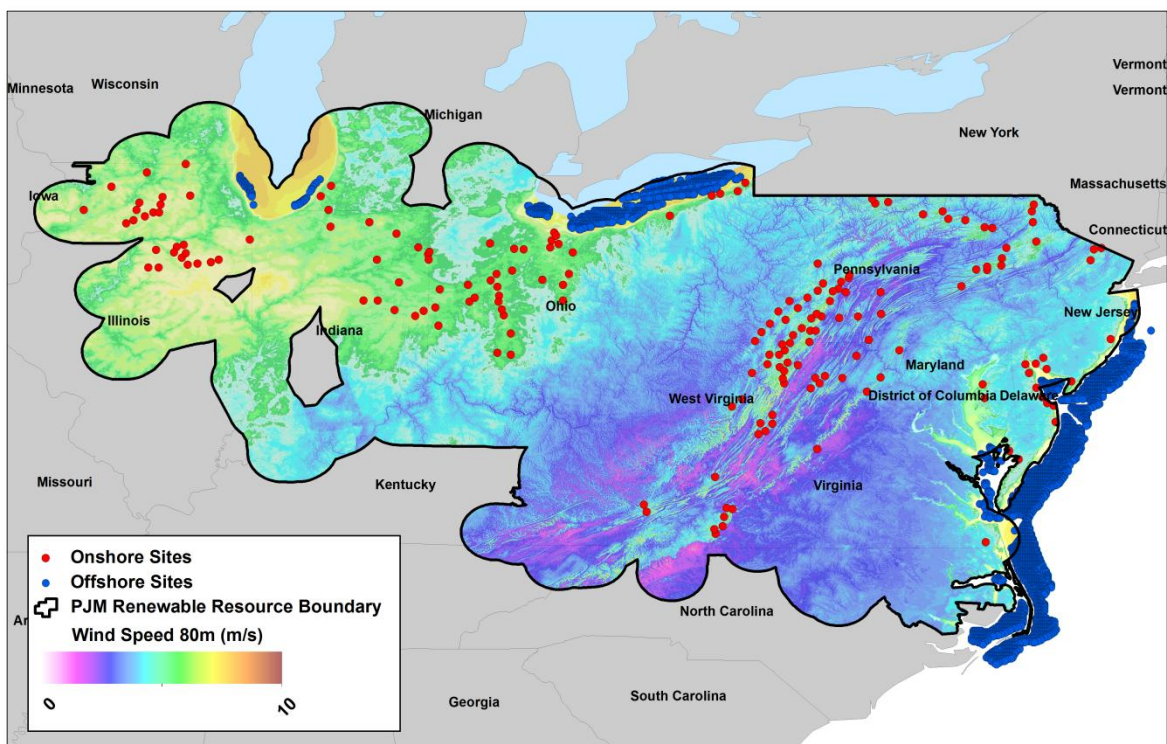
Figure 3. Selected onshore and offshore wind sites with annual average wind speed at 80 m height.

3.2. SOLAR

Solar power plants were selected in a similar way to that of wind. A prerequisite for the solar site selection was to create a solar resource map for the PJM Service Territory. The three year EWITS meteorological dataset was used to compute a solar resource map for the PJM Service Territory. The same exclusion areas that were used in the wind site screening were applied for the solar site screening, except that the slope exclusion was modified to 10%. The solar site selection was primarily based on annual net energy output and cost of energy. In July 2011, after completing the initial sites screening for solar sites in the PJM region, a stakeholders meeting was held to discuss the results. It was determined that in order to meet requirements for a 30% RPS scenario, the solar site screening should be expanded significantly to reach 74 GW from centralized and distributed solar power plants.

3.2.1. Centralized

The centralized site screen was completed using AWST's internal software application to select suitable PV generation facilities. The program operates in two main steps. In the first, it finds all sites with a maximum output in the immediate vicinity (i.e. a local maximum) with sufficient area to support a project of the desired range. For the PJM region, the range was set to 10–100MW rated capacity. In addition, sites were spaced no closer than 25 km from any neighboring site. In the second step, the program allows each of these sites to expand so long as the output does not decrease by more than 5%. If the site encounters another site, the site that has a higher mean output is retained and the other is dropped.

To meet the GE defined solar capacity requirements in states with lower solar resource, AWST allowed the number of solar power plants per area to increase, setting the minimum spacing to 10 km for DE, IL, OH, and NJ. This effectively increased the density of sites in these states. Selected hypothetical centralized solar plants are shown in Figure 4, where a given site capacity is represented by the size of the red dots. A total of 2099 utility-scale solar power plants with a capacity of 63.81 GW were selected from the PJM Service Territory. The plant rated capacity ranged from 10 – 150 MW, with most plants ranging from 10 – 15 MW (Figure 5). Additionally, 354 planned and existing plants totaling 4.08 GW are included in the analysis (Table 3).
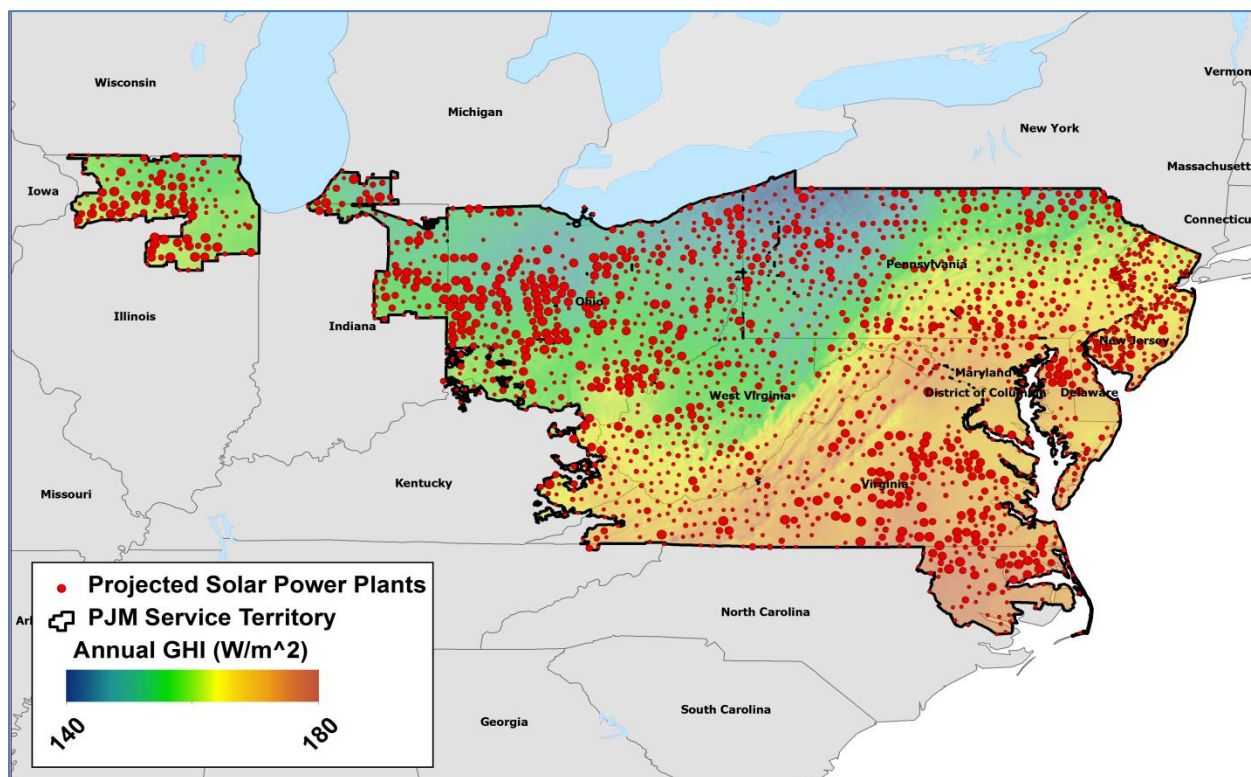
Figure 4. Selected centralized solar power plants with annual average solar irradiance within the PJM Service Territory.

Projected and Planned Utility Sites
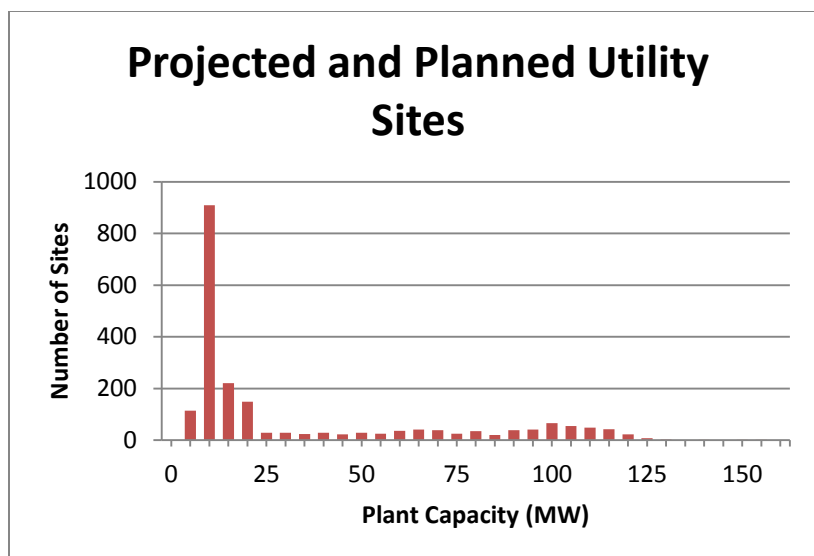
Figure 5. Capacity of centralized solar power plants.

Table 3. Centralized solar power plants for all planned and projected sites.

State	Plants in Queue	Queue Capacity (GW)	Projected Plants	Projected Capacity (GW)	Total Plants	Total Centralized Capacity (GW)
DC	0	0.00	0	0.00	0	0.00
DE	1	0.01	15	0.47	16	0.48
IL	4	0.05	123	5.78	127	5.84
IN	0	0.00	68	2.82	68	2.82
KY	0	0.00	50	1.41	50	1.41
MD	9	0.12	73	2.27	82	2.39
MI	0	0.00	22	0.99	22	0.99
NJ	265	2.67	49	1.09	314	3.75
NC	4	0.07	70	2.54	74	2.61
OH	14	0.22	364	18.45	378	18.67
PA	47	0.76	409	11.76	456	12.52
TN	0	0.00	2	0.08	2	0.08
VA	10	0.19	300	11.51	310	11.70
WV	0	0.00	200	4.63	200	4.63
Total	**354**	**4.08**	**1745**	**63.81**	**2099**	**67.89**

3.2.2. Distributed

Whereas specific sites were chosen for centralized PV plants, all urban areas within the PJM Service Territory (as defined by the Environmental Systems Research Institute database of United States cities) were considered as opportunities for distributed PV systems. Within each city, the United States

Geological Survey's National Land Cover Database (NLCD) classifications were used to determine the portion of each city suitable for commercial versus residential solar PV development. The assumptions used to estimate each city's maximum commercial and residential PV capacity are detailed in Table 4.The cities were then ranked by the mean annual irradiance. Although many factors such as available land area, solar resource, economic incentives, and government initiatives will ultimately impact the percentage of available area that will be developed, for the purposes of this study it was assumed that a greater percentage of the available potential will be developed in cities with greater average irradiance resource (Figure 6).These assumptions were adjusted until the required total distributed generation capacity, capacity requirements per state, and suggested mix of residential and commercial rooftop PV were met.

Table 4. Distributed solar capacity assumptions.

NCLD Classification	Description	Site Classification	Capacity Assumption (W/km^2)
24	High Intensity	Commercial	5556
23	Medium Intensity	Residential	2778
22	Low Intensity	Residential	277
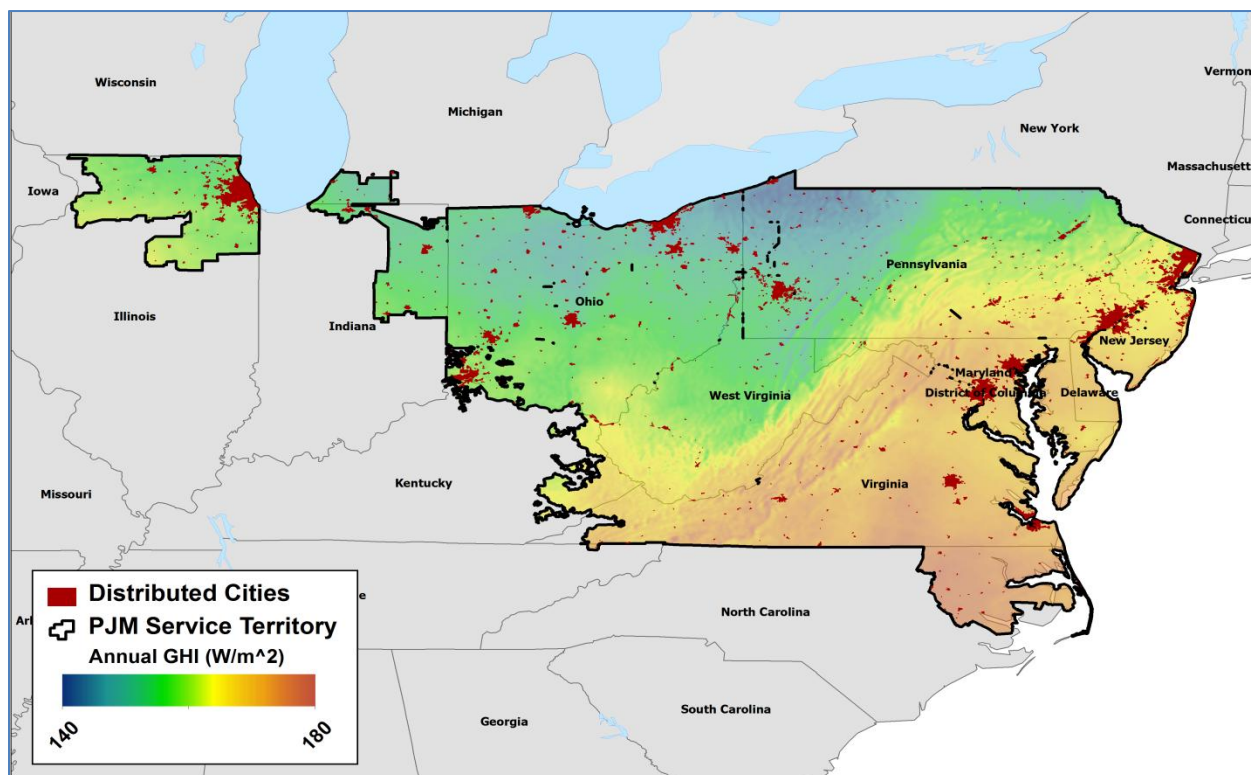
Figure 6.Selected distributed cities with annual average solar irradiance within the PJM Service Territory.

AWST suggested a mix of residential and commercial rooftop PV based on solar plants in the PJM queue and data from the PJM Environmental Information Services (EIS) Renewable Generator List.[3] The PJM EIS Renewable Generator List includes 17222 existing PV units (70 W to 18.29 MW in size) within the PJM Control Area and surrounding regions. Although there is some variation by state, likely due to such factors as available land area, solar resource, and economic incentives, the data support a mix of roughly 20% residential and 80% commercial rooftop PV. The AWST distributed site screening process attempted to first match this overall mix of sites, while meeting the required percentages by state was a secondary priority. The breakdown (Table 5) results in 51.85 GW of rooftop PV, which is approximately 70% of the total distributed generation capacity required for the superset.

Table 5. Mix of residential and commercial rooftop solar power by state.

State	# Cities	Residential GW	%	Commercial GW	%	Rooftop Target (70%)	Total GW
DC	1	0.30	16%	1.58	84%	0.03	1.89
DE	8	0.23	39%	0.36	61%	0.36	0.59
IL	91	1.61	16%	8.47	84%	1.27	10.08
IN	27	0.12	13%	0.86	87%	0.00	0.98
KY	6	0.03	18%	0.16	82%	0.00	0.19
MD	44	0.90	26%	2.58	74%	1.12	3.48
MI	17	0.02	15%	0.11	85%	0.00	0.13
NC	24	0.04	22%	0.16	78%	0.01	0.20
NJ	99	4.06	31%	8.98	69%	3.54	13.04
OH	201	1.39	18%	6.38	82%	0.66	7.77
PA	285	1.22	13%	8.44	87%	0.64	9.66
TN	2	0.00	19%	0.00	81%	0.00	0.00
VA	91	0.42	13%	2.73	87%	0.00	3.16
WV	52	0.10	15%	0.56	85%	0.00	0.67
Total	**948**	**10.47**	**20%**	**41.38**	**80%**	**7.64**	**51.85**

4. GENERATION OF POWER PROFILES

4.1. WIND

Time series of meteorological variables were extracted from each mesoscale model grid point associated with a wind plant site. An internal software application written by AWST was used to convert the meteorological fields to wind power.

The program starts by reading a list of four validation towers within the PJM region and their nearest associated EWITS grid cell information. It also reads a list of the grid cells associated with each site. Up to several dozen grid cells are associated with each site, depending on its size and shape. For each cell, the list provides the latitude and longitude, expected mean speed of the part occupied by turbines, mesoscale elevation, actual mean elevation of the turbines, and relative proportion of the site's total rated capacity associated with that cell. The mean speeds are based on AWST's wind maps adjusted to

---

[3] https://gats.pjm-eis.com/myModule/rpt/myrpt.asp?r=228

the year of the simulation for the selected hub heights of 80 m and 100 m. Each year was modeled based on the ratio of the long term average to that year's mean wind speed allowing AWST to capture the high resolution grid scale wind variability while maintaining the long term statistical mean of the site's wind speed.

The software application then imports power curves for the turbines to be modeled. The power curve represents the average power output that would be expected from an industry standard wind turbine based on the appropriate International Electrotechnical Commission (IEC) class. In order to account for advances in turbine technology since the EWITS data sets were created, the composite power curves used in that study were updated with larger, more powerful turbines likely to be used for future wind farms. Table 6 describes the inputs used to create the composite curve and Table 7 gives the actual curves used for power conversion. Due to differences in cut-out speeds of included turbines, a standard cut-out speed of 22 m s^{-1} and 25 m s^{-1} was selected for the IEC-3 and offshore composites. The power curves are scaled to a rated capacity of 2 MW and are valid for the standard sea-level air density of 1.225 kg/m^3. The software adjusts the curves based on the air density computed from the modeled temperature and pressure. IEC-1 and IEC-2 composites were used at 80-m hub height, while IEC-3 and the offshore composite were used at 100 m.

Table 6. Wind turbines used to create composite, categorized by IEC class.

Turbine	Rated Power (MW)	Cut-in (m/s)	Max Power (m/s)	Cut-out (m/s)
Class I				
Siemens 3.0MW	3	3	14	25
Gamesa G80	2	4	17	25
Nordex N90HS	2.5	4	14	25
Vestas V90	3	4	14	25
Class II				
Vestas V112	3	3	13	25
Siemens 2.3MW	2.3	3	13	25
GE1.6 82.5	1.6	4	12	25
GE2.5xl	2.5	3	14	25
Class III				
Vestas V100	1.8	3	12	20
GE1.6-100	1.6	3	12	25
Repower 3.2M	3.2	3	12	22
Offshore				
Siemens 3.6MW	3.6	4	14	25
GE4.1MW	4.1	4	14	25
Repower 6M	6.15	3.5	14	30

Table 7. Updated composite power curves.

Speed	IEC - 1	IEC - 2	IEC - 3	Offshore
0	0	0	0	0
1	0	0	0	0
2	0	0	0	0
3	0.0043	0.0052	0.0054	0
4	0.0323	0.0423	0.053	0.0281
5	0.0771	0.1031	0.1351	0.074
6	0.1426	0.1909	0.2508	0.1373
7	0.2329	0.3127	0.4033	0.2266
8	0.3528	0.4731	0.5952	0.3443
9	0.5024	0.6693	0.7849	0.4908
10	0.6732	0.8554	0.9178	0.6623
11	0.8287	0.9641	0.9796	0.815
12	0.9264	0.9942	1	0.9179
13	0.9774	0.9994	1	0.9798
14	0.9946	1	1	1
15	0.999	1	1	1
16	0.9999	1	1	1
17	1	1	1	1
18	1	1	1	1
19	1	1	1	1
20	1	1	1	1
21	1	1	1	1
22	1	1	1	1
23	1	1	0	1
24	1	1	0	1
25	1	1	0	1

There are several additional components that are used in the software application that take into account physical constraints of wind power generation and other predicted losses. Since the methodology used for EWITS was replicated for this study, further details of the power conversion process and loss assumptions can be found in the EWTIS Technical Report[4].

For each site, the simulated wind speeds at 80 and 100 m and the power output for all IEC classes are output to a single text file. In addition, the software selects most appropriate IEC class based on the estimated maximum long-term annual average mean speed within the site, adjusted for air density. The power output for the selected IEC class is provided in the last column of the file. In this way, users of the data can simply import the last column rather than have to select themselves which IEC class to use. All timeseries data is delivered in Greenwich Mean Time (GMT).

In review of the data, the study team discovered discontinuities in the diurnal variability when the power output from several wind farms was aggregated. This pattern is likely due to observed measurements that are ingested into the mesoscale simulations every 12 hours (0000 and 1200 UTC) to

realign the model with actual conditions. Although several techniques were employed to mitigate the effect at individual wind farms, the problem was still apparent in the aggregate of both onshore and offshore sites. A new correction was developed to adjust the correlated component of the wind power fluctuations by adding a proportion of the adjustment to each individual site. To facilitate the use of the adjustment for future studies, the onshore sites from EWITS were adjusted for the aggregate of the EWITS sites within PJM, the queue sites were adjusted for the queue site aggregate, and the offshore sites were adjusted for the offshore aggregate. In this way, the diurnal discontinuity in the aggregate was adjusted (Figure 7) while only small changes were made at each site (Figure 8). The initial adjustment was found to increase the energy at each site due to a rounding error. This issue was addressed, and the final diurnal adjustment was found to produce total energy similar to the originally delivered data at each site (Figure 9). Although the 12-hour data assimilation problem was addressed, an hourly signal remained. The study team determined that the hourly fluctuations were acceptable for this project.
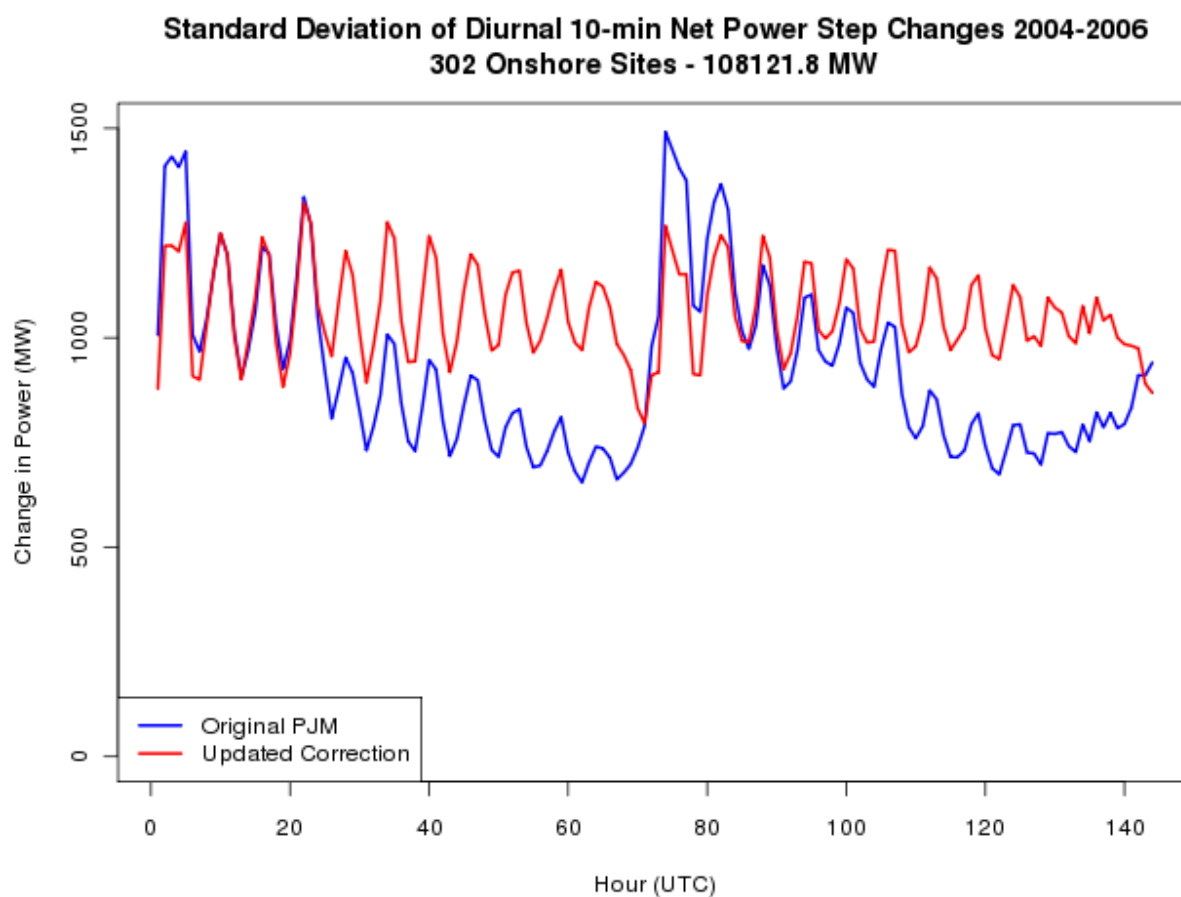
Figure 7. Diurnal mean standard deviation of 10-minute net power deltas from 302 onshore sites before (blue) and after (red) the diurnal correction was applied.

Onshore Site: 671 Capacity: 100.1 MW
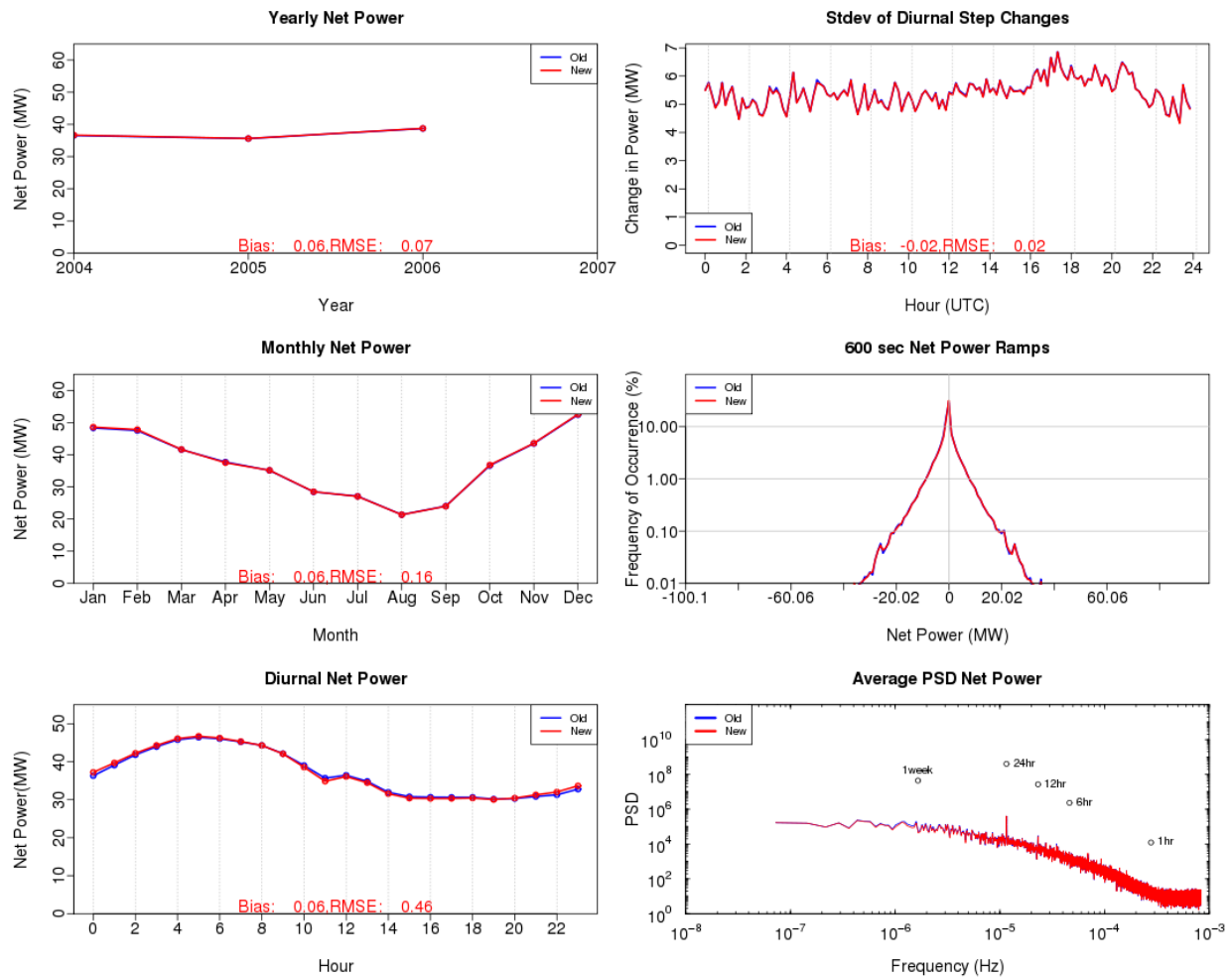
Figure 8. Comparison of net power at a sample onshore site before (blue) and after (red) the diurnal adjustment. The left panels depict annual, monthly, and diurnal means, while the right panels show the diurnal mean variability, frequency distribution of 10-minute ramps, and power spectral density.

PJM Onshore Sites
Ratio New to Old
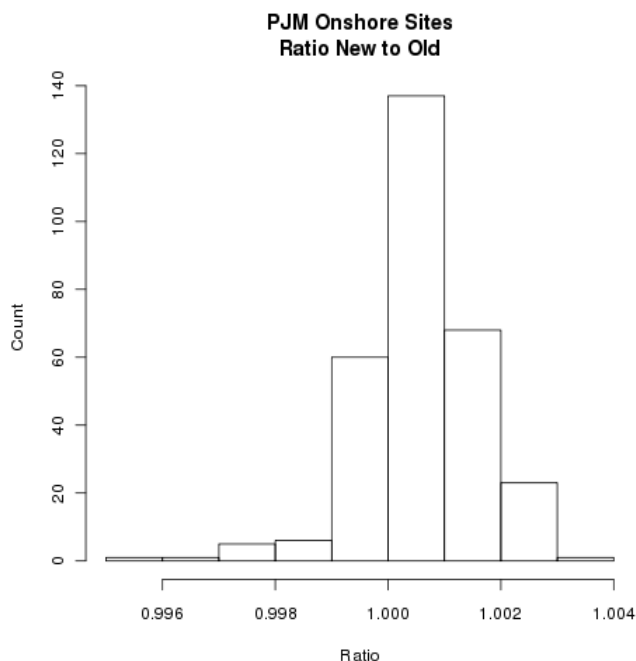
Figure 9. Histogram of the ratio of energy from PJM onshore wind sites as originally delivered versus after the diurnal adjustment.

In summary, the final PJM wind data set includes several updates from the original EWITS data:

- Winds were scaled to updated mean map speeds based on additional validation since 2008
- Diurnal patterns were scaled to additional tall tower measurements available
- Power curves were updated with larger, more powerful turbines
- Diurnal variability was adjusted to minimize the impact of data assimilation

4.2. SOLAR

The conversion of solar power output was completed using the modeled irradiance data from the EWITS and several software applications developed by AWST. The power conversion process was similar for both centralized and distributed sites. The main difference was the specific module technology and orientation used for the power output calculation. The following steps were used to compute power output.

The three year time series of 10-minute output was extracted from the raw MASS modeled data at each grid cell associated with the centralized and distributed sites. The following variables impacting module performance and power conversion were extracted – global horizontal irradiance (GHI) (W/m^2), temperature at 2 m above ground level (°C), specific humidity at 2 m above ground level (g/kg), wind speed at 10 m above ground level (m/s), rain (mm), snow (mm), and freezing rain (mm). These data were stored in comma delimited format denoted by the EWITS grid number and grid cell coordinate.

In previous comparisons with observed data, it was determined that the MASS model underestimates cloudiness, resulting in a model high bias for GHI (i.e., modeled mean greater than observed mean). Since these analyses show no obvious pattern in the bias distribution across the region, it was decided to adjust the modeled 10-minute GHI to match the frequency distribution of GHI observations within and surrounding the PJM region. This process adjusts both the means and the extremes to observed

values, and results in a more accurate representation of clear, partly cloudy, and cloudy days. The adjustment effectively eliminates the monthly bias at all six validation stations and reduces the root-mean-square error (RMSE) from 62.1W/m^2 to 7.2 W/m^2. The effect of the adjustment on diurnal and monthly mean GHI at a sample station is shown in Figure 10 and Figure 11, respectively.

PennState_PA Hourly Global
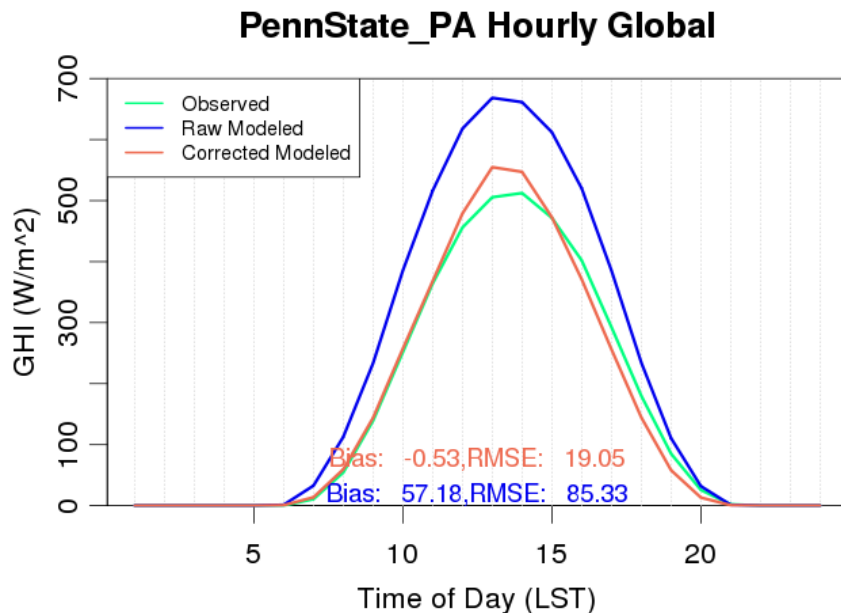
Figure 10. Hourly averaged global horizontal irradiance for the Penn State observation station.

PennState_PA Monthly Global
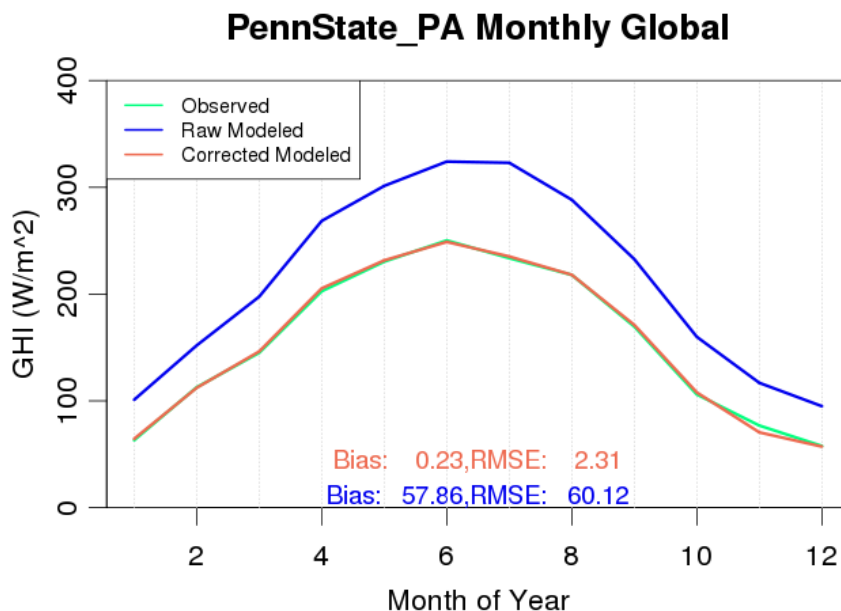
Figure 11. Same as Figure 10 except monthly average.

In addition to knowing the GHI, or total solar irradiance, the components of irradiance are also necessary to compute solar PV output. Direct normal irradiance (DNI) is the amount of light coming

directly from the sun, unscattered by clouds and atmospheric aerosols, and impinging on a surface perpendicular to the sun's rays. Diffuse horizontal irradiance (DHI) is the solar radiation scattered and reflected from the rest of the sky due to clouds and aerosols and striking a horizontal surface. Since the DNI and DHI components were not stored in the original EWITS data, they were partitioned from the MASS adjusted GHI. Stations with observed irradiance components within and surrounding the PJM region were used to develop a relationship between DHI and GHI for each hour of the day and month of the year. This relationship was then applied to the modeled data, and the resulting irradiance components were replicated with reasonable accuracy. In this way, a complete three-year time series of all irradiance components was generated. Composite PV modules consisting of several current technologies and manufacturers were created to represent possible configurations of centralized and distributed sites. The composite modules were determined using technical data available as of July 2011. The resulting module parameters are given in Table 8.

The power conversion process proceeded from this point with the following steps:

- The number of PV modules necessary to reach a site's presumed rated capacity was calculated using the composite module rated capacity. The PV area was then calculated by multiplying the number of modules by the composite module area. This area was then used in the power output calculations.
- Gross power output was obtained by multiplying the PV area by the plane-of-array global irradiance and composite module efficiency.
- The standard loss assumptions included in the net energy calculations are listed in Table 9.
- Shading losses were varied by time of day based on module spacing.
- Soiling losses varied based on precipitation. Soiling losses were decreased after significant rainfall and increased after snow accumulation.

Table 8. Composite PV module characteristics.

Module Characteristic	Composite Thin Film	Composite Crystalline
Nominal Power (W) (+/-5%)	77.50	220.00
Voltage at P_{max}	58.19	28.20
Current at P_{max}	1.38	8.00
Temperature Coefficient (%/°K)	-0.25	-0.46
Efficiency (%)	10.76	13.85
Area (m^2)	0.72	1.55

Table 9. Loss Assumptions for PV sites. Although losses will vary by site and location in actuality, representative values for the PJM region were chosen for this study.

Loss Source	%
Module Mismatch	1.50
Module Quality	2.00
Soiling*	3.00–5.00
Inverter Efficiency**	1.50
Availability of System and Substation	1.00
DC wiring	1.00

AC wiring	1.00
HVAC and Auxiliary Components	0.02
Transformer	1.00
Non-STC Operation (Irradiance)	2.00
Near Shading***	3.00-4.60
Degradation	0.6%/year

*Losses due to snowfall are additional
**Losses due to temperature outside of inverter operating range (-20°C to 50°C) are additional
***Varies based on latitude, module spacing, and time of day; horizon shading is not considered

4.2.1. Centralized

All of the selected and planned solar generation facilities greater than 1 MW in nameplate capacity were modeled as centralized sites. All inputs used for the power conversion were discussed with the stakeholders and were selected as being representative of future sites. The following assumptions or specifications were used as input to the power conversion procedure:

- Power was modeled with both thin-film and crystalline PV technologies, each represented as composites of common manufacturers and types.
- Two system types were considered: single axis tracking with a north-south axis (tracks east-to-west), oriented due south, and fixed tilted at latitude, oriented due south.
- Single axis tracking systems were modeled with crystalline PV, while fixed systems were modeled with thin-film.
- A ground cover ratio (actual module area/total area) of 0.35 was used for single axis systems. A ground cover ratio of 0.4 was used for fixed systems.

4.2.2. Distributed

All of the distributed residential and commercial city locations were modeled using the same process as centralized sites, with the exception of module parameters and system types. The following specifications were used as input for power conversion:

- Since it was assumed that larger systems would be optimally configured, commercial systems were modeled with the PV modules tilted to latitude and oriented due south.
- To account for the range of module tilt and orientations expected across a city, an average of two tilt angles and three azimuth angles were chosen for residential distributed sites. A common roof pitch for the eastern U.S. (30°) and the site latitude were used as the tilt angle, while 180°, 210°, 150° from N were used for the azimuth angle. These independent simulations were then averaged together to form a single residential PV profile per city. The effect of aggregating these configurations is shown by the diurnal mean profiles in Figure 12.
- Residential and commercial sites were modeled as a crystalline technology developed from a composite of common manufacturers and types.
- Losses due to temperature outside of inverter operating range were not considered for distributed sites, as it was assumed that the inverter might be housed indoors and protected from adverse temperature conditions.
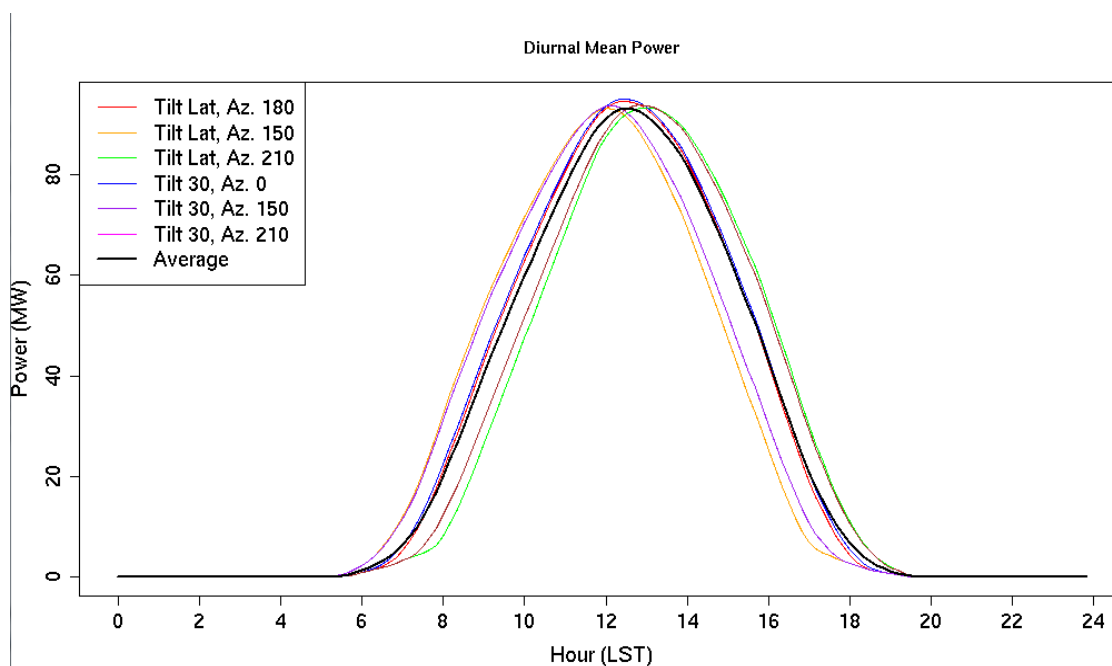
Figure 12. Diurnal mean power at a sample location for each tilt and azimuth combination used for distributed PV. The average of all profiles is shown by the black line.

5. FORECASTS

5.1. WIND

Although wind forecasts were part of the original EWITS data set, it was determined that new forecasts would be created using the updated power curves and actual power generation data from plants within the PJM region. AWST produced hourly forecasts for three different time horizons: next-day, six-hour, and four-hour ahead. Each set of forecasts was synthesized by running a statistical forecast synthesis tool called SynForecast, which was developed by AWST. This tool uses actual forecasts and observed plant output to develop a set of transition probabilities. The probabilities are applied to simulated plant output data, stepping forward in time from a random starting point in a process known as a Markov chain. This process results in a synthetic forecast that imitates the statistical behavior of a real forecast. The procedure is described in depth for wind and solar.

The first step in the forecast synthesis process is to produce a sequence of real forecasts for one or more operating wind projects using a state-of-the-art wind forecasting system. It is assumed that these forecasts are typical or representative of what forecasts would look like at other sites in the region. For this purpose, AWST obtained power forecasts and observed output from 30 wind plants within the PJM region. Due to various inconsistencies in the forecast data provided by PJM, including mismatched plant capacities (additional installed capacity during the two years), excessive curtailments, or incomplete period of records, 12 wind plants were removed from the analysis. The remaining sites were processed through the eWind® forecasting system[5] which was executed in "hindcast" mode for one full year

---

[5] eWind® is a state-of-the-art commercial wind power forecasting service. It takes as its main inputs weather forecasts from a mesoscale weather model and actual plant operating data; on-site wind observations are also often used. Over a period of several days or weeks, eWind builds a statistical model relating the forecasted plant

(2010). The mesoscale model feed for the *eWind* forecasts were provided by 8-km resolution MASS simulations. The observed data feed was provided by the actual plant data up to the time each forecast was assumed to be generated. For the next-day forecasts, this was 5 pm local time of the day before the forecast; this effectively assumes the forecasts are generated once per day. For the four-hour and six-hour forecasts, the latest time was four hours and six hours ahead of the delivery time, which implies an hourly update schedule. Analysis of the *eWind* forecasts showed the mean absolute error of the hindcast data to be noticeably lower than the observed forecasts provided by PJM. In order to avoid creating forecasts whose errors are too low, two years of actual forecasts (July 2009–June 2011) and observations was used in the SynForecast program.

From each of these three sets of forecasts, the SynForecast program constructed a matrix of forecast probabilities of the following form:

$$P(A_t \cap F_{t-1} \cap F_t)$$

The probability *P* is the number of occurrences for which the actual output was A_t and the forecasted outputs were F_{t-1} and F_t, where *t* is a particular moment in time and *t-1* is the previous moment (one hour earlier). Before constructing this matrix, both the actual and forecasted output values were normalized to the rated capacity of the wind project and placed in 10 bins ranging in capacity factor from 0.05 to 0.95 in increments of 0.10. Both the current and previous forecasts were included in the probability matrix to capture the autocorrelation of forecast errors, as otherwise the synthesized forecasts would fluctuate randomly about the actual output in an unrealistic fashion.

For each wind project site, the SynForecast program selected, at random, one of the 18 transition probability matrices. Both onshore and offshore projects made use of the same 18 matrices since given the lack of offshore plant output data, it is not known whether forecast skill will be similar for offshore projects as for onshore projects. Starting with a random seed, the program stepped forward in time taking random draws from the transition matrix. In this manner, an hourly next-day forecast was synthesized.The same procedure was followed for 4 and 6 hour-ahead forecasts.

The wind power forecasts were updated with the wind power diurnal variability adjustment, which produced no appreciable change in the forecast correlations and error statistics.

5.2. SOLAR

In the absence of actual solar plant output data for the PJM region, AWST produced hourly irradiance forecasts for three different time horizons: next-day, six-hour, and four-hour head. The SynForecast program was augmented to reproduce the statistical behavior of solar forecasts. This tool uses actual irradiance forecasts and observed solar irradiance profiles to develop a set of transition probabilities.

The first step in the irradiance forecast synthesis process is to produce a sequence of forecasts for several observed solar observation stations using the AWST solar forecasting system. AWST obtained solar irradiance profiles from 6 geographically diverse observation sites. These data were processed through the AWST solar forecasting system. This system was executed in "hindcast" mode for three full years (2004-2006). The mesoscale model feed for the AWST solar forecasting systemwas provided by 8-km resolution MASS simulations. The observed data feed was provided by the actual irradiance profiles up to the time each forecast was assumed to be generated. For the next-day forecasts, this was 5 pm

---

output to the actual plant output. This model is then applied to correct the wind forecasts going forward. Over time, the model "learns" from past forecast errors, and its skill gradually improves.

local time of the day before the forecast; this effectively assumes the forecasts are generated once per day. For the four-hour and six-hour forecasts, the latest time was four hours and six hours ahead of the delivery time, which implies an hourly update schedule.

Before constructing the probability matrices, both the actual and forecasted irradiance values are normalized to the maximum possible irradiance values for that particular hour and day of the year.These values were then placed in 10 bins ranging from 0.05 to 0.95 in increments of 0.10 (% of maximum irradiance).

For each solar project site, the SynForecast program selected, at random, one of the 6 transition probability matrixes. Starting with a random seed, the program stepped forward in time taking random draws from the transition matrix. In this manner, an hourly next-day forecast was synthesized.The same procedure is followed for 4 and 6 hour-ahead forecasts.The corresponding irradiance forecasts where then converted to power following the procedure outlined in Section 4.2. The steps used to compute PV forecasts were similar for both centralized and distributed sites.

6. VALIDATION

Each of the delivered datasets underwent a detailed validation process to ensure the results were consistent with actual meteorological and power generation observations. AWST used as much publicly and privately available observed data as possible at the time of the study. This included four publicly available tall tower measurements, wind power output from 18 generation facilities, and six publicly available solar monitoring stations containing measurements of the three components of solar radiation. Each of these data sources was independently validated against the modeled data to determine the accuracy of the provided datasets.

6.1. WIND

6.1.1. Power Generation

The wind power validation consisted of making direct comparisons with actual power generation data for eight of the power plants in the PJM region. The eight sites used for validation contain actual wind turbine layouts with specifications for turbine type, hub height, and total plant capacity. These layouts were used to model each actual facility in the same manner as the projected sites. Using the specified wind turbine model from each facility, power generation profiles were created for the period of 2004–2006. Although special care was taken to ensure consistency between the observed and modeled data, observed generation data were only available from February 2009 to July 2011. Therefore, the period of record does not overlap in time, leading to some discrepancy in the validation. The datasets were merged to the same length of time, i.e. from February 2009–July 2011 and from February 2004–July 2006.

A reasonable agreement was found between all of the modeled and observed plants. The total capacity factor bias ranged 0.4% to 10.1% (Table 10). The large difference in capacity factor at Mill Run was attributed to the mountainous region were the plant is installed and the difficulty in associating individual turbine locations with modeled grid cells. The time averaged profiles were compared at all sites and were found to be generally agreeable. Results at the Crescent Ridge facility are shown in Figure 13. Monthly and diurnal mean profiles are shown in Panel 1 and Panel 2, respectively. The modeled and observed ramp frequencies (step change frequency as a function of step change size) for each modeled location for 10-minute (Figure 13, Panel 3) and 60-minute (Figure 13, Panel 4) intervals were also

computed. The ramp rates for each modeled point are quite similar on both time scales, with some difference at step changes larger than 50% of plant capacity. The modeled data appear to be slightly less variable than the observed in most cases for such large changes. Lastly, the power spectral density (PSD) was computed for each plant (Figure 13, Panel 5). The PSD gives an indication of the power (square of the amplitude) of fluctuations at different frequencies. The model shows good agreement with the observed at all scales, particularly at frequencies greater than 10^{-7} Hz (periods of less than about one minute).

Table 10. Summary of modeled versus observed capacity factor bias (observed – modeled) for eight onshore wind facilities in the PJM region.

Location	Bias
Camp Grove	0.059
Crescent Ridge	-0.004
Forward	0.030
Highland	0.032
Lookout	0.062
Mendota Hills	-0.078
Mill Run	0.101
Providence Heights	-0.007
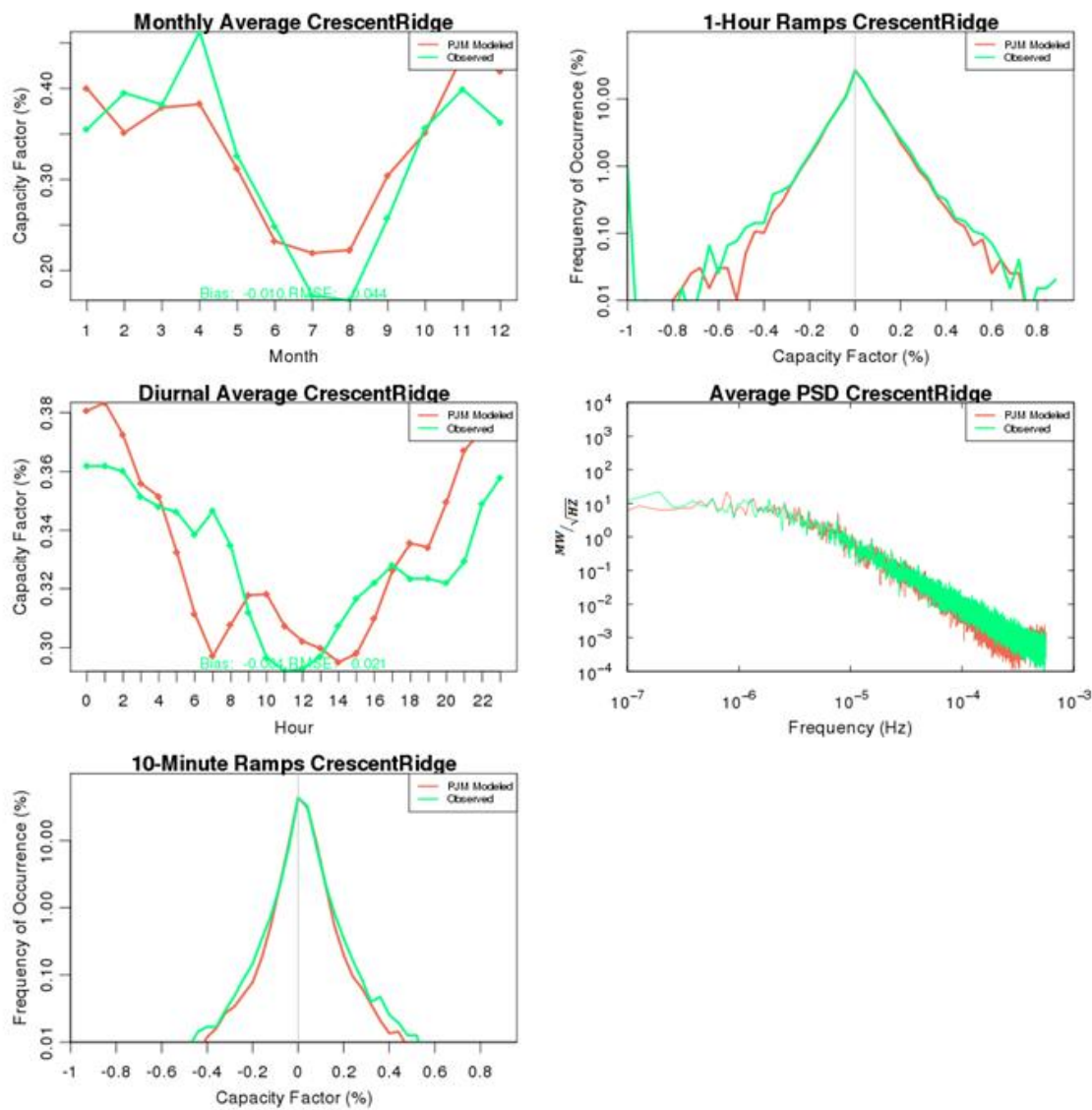
Figure 13. Comparison of modeled versus observed power generation at Crescent Ridge. Reading down then across, panel 1 is the monthly averaged power output with the modeled shown in red and the observed shown in green; panel 2 is the same as 1 except for the diurnal cycle; panel 3 is the 10-minute step change in power output as a percentage of plant capacity; panel 4 is the same as 3 except for 1-hour step changes; and panel 5 is the power spectral density of power output.

The same comparison was made for each of the eight modeled generation facilities. Results for Providence Heights are shown in Figure 14. Given that the periods of record do not contain data from the same years, there was some discrepancy in the monthly and diurnal profiles. The high bias in the summer months was found to be an artifact of the difference in wind speed between the periods compared, and not the power conversion process. This was determined to be acceptable as the modeled and observed wind speeds from coincident time frames coincide very well, particularly in regions of less complex terrain, i.e. in the Midwest.
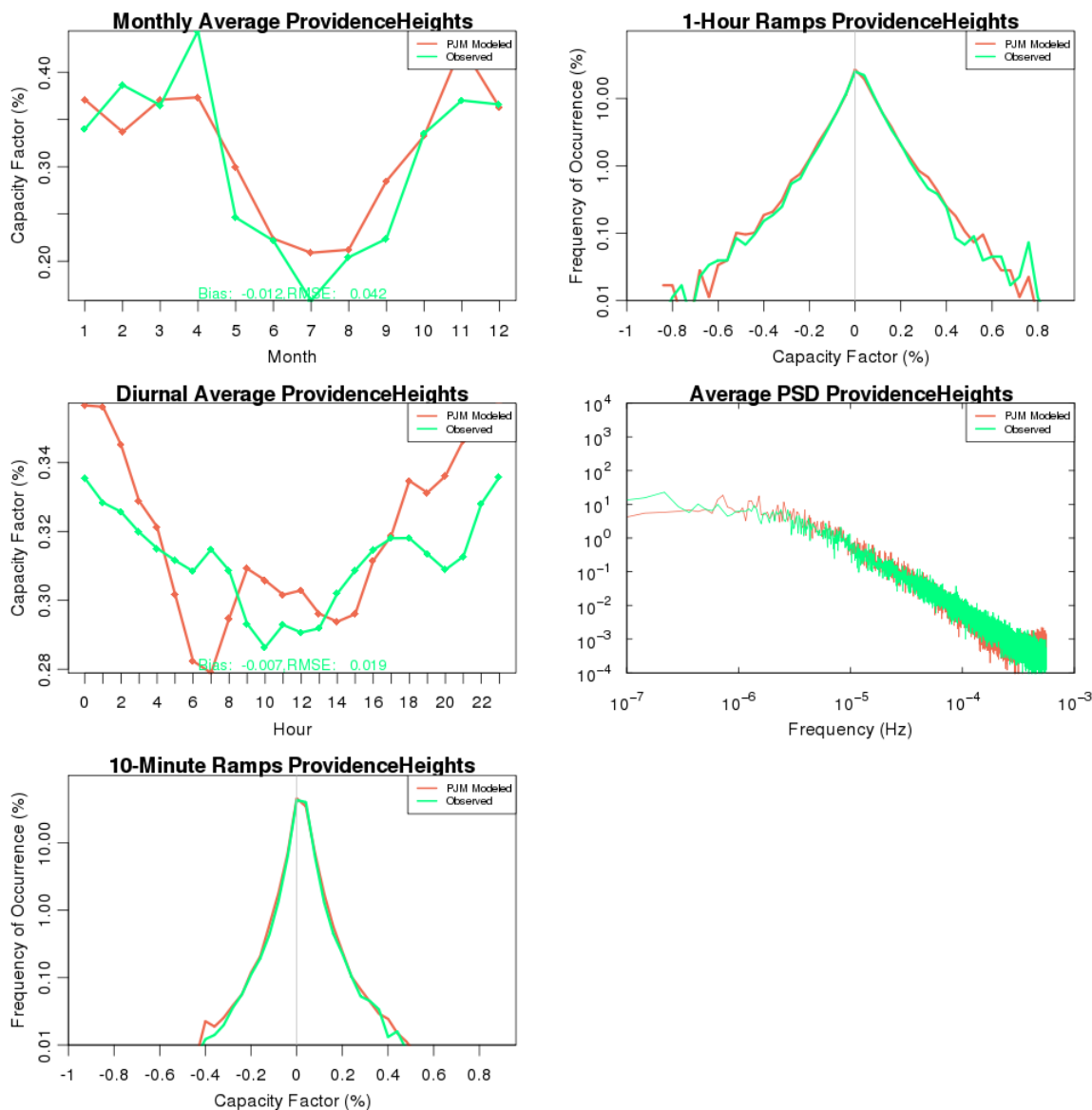
Figure 14. Same as in Figure 13, except for at the Providence Height wind generating facility.

6.1.2. Forecasts

To verify the accuracy of the synthetic wind forecast, AWST compared synthesized forecasts with the actual forecasts for the 18 validation wind projects. First, the time correlation of the actual and forecasted generation, root-mean-square, and mean absolute (MAE) forecast error were considered for all proposed forecast time horizons. The results of the actual and synthesized forecasts were very similar, as shown by the next-day statistics in Table 11. The RMSE depends in part on the average plant output, with more productive plants experiencing greater forecast errors as a fraction of rated capacity because they spend more time in the steeply sloping parts of their power curves.

Next, the autocorrelation of the output, the forecasts, and the forecast errors was considered. The autocorrelation indicates the degree to which a particular parameter tends to persist over time. A parameter that typically changes little would have an autocorrelation factor of nearly one, whereas one that fluctuates randomly would exhibit an autocorrelation factor of nearly zero.

Table 11. Next day wind forecast capacity factor correlation, RMSE, and MAE.

Next Day Forecast	Correlation (R)		RMS Error		MA Error	
Power Plant	PJM	SynFcst	PJM	Synfcst	PJM	Synfcst
Backbone Mountain	0.768	0.678	0.23	0.237	0.167	0.18
Bear Creek	0.695	0.636	0.234	0.238	0.16	0.172
Camp Grove	0.826	0.796	0.175	0.185	0.121	0.133
Crescent Ridge	0.79	0.735	0.186	0.198	0.129	0.146
Forward	0.825	0.813	0.158	0.155	0.106	0.111
Greenland Gap	0.759	0.688	0.203	0.21	0.141	0.155
Highland	0.726	0.705	0.193	0.187	0.128	0.131
Locust Ridge	0.787	0.76	0.205	0.206	0.146	0.156
Locust Ridge II	0.778	0.797	0.165	0.158	0.114	0.115
Lookout	0.803	0.778	0.203	0.205	0.142	0.151
Mendota Hills	0.76	0.746	0.148	0.149	0.099	0.106
Mill Run	0.681	0.659	0.223	0.218	0.15	0.163
Old Trail	0.813	0.77	0.198	0.207	0.14	0.153
Providence Heights	0.72	0.747	0.198	0.184	0.137	0.137
Waymart	0.792	0.719	0.184	0.207	0.126	0.152
West Brooklyn	0.755	0.724	0.191	0.196	0.131	0.145
EcoGrove Wind	0.777	0.779	0.182	0.18	0.125	0.133
High Trail	0.813	0.773	0.192	0.201	0.133	0.147

Table 12 demonstrates how well the synthetic forecast compares to the actualwind project forecast. It was found that the forecast tends to be quite strongly autocorrelated over a period of one to a few hours (Figure 15). The actual and synthesized forecasts exhibit similar degrees of autocorrelation in each case. The autocorrelation of forecast errors is considerably lower, and the SynForecast program seems to capture the pattern of decreasing correlation with increasing time shift quite well. However, the synthesized forecasts are slightly more correlated in time than the actual forecasts for the next day time horizon, which affirms that the synthesized forecasts are more dependent on the numerical simulation as the forecast time increases.

Table 12. Bear Creek autocorrelation of wind forecasts and forecast error (Pearson R Correlation).

Time Shift (h)	Observed	PJM	Synfcst	PJM Error	Synfcst Error
0	1	1	1	1	1
1	0.944	0.980	0.959	0.890	0.921
2	0.875	0.946	0.924	0.769	0.842
3	0.814	0.906	0.888	0.674	0.772
4	0.756	0.863	0.852	0.600	0.706
5	0.700	0.820	0.817	0.536	0.644
6	0.647	0.776	0.784	0.484	0.589
7	0.598	0.733	0.751	0.437	0.535
8	0.552	0.691	0.719	0.399	0.487

Bear_Creek - Next Day Autocorrelations
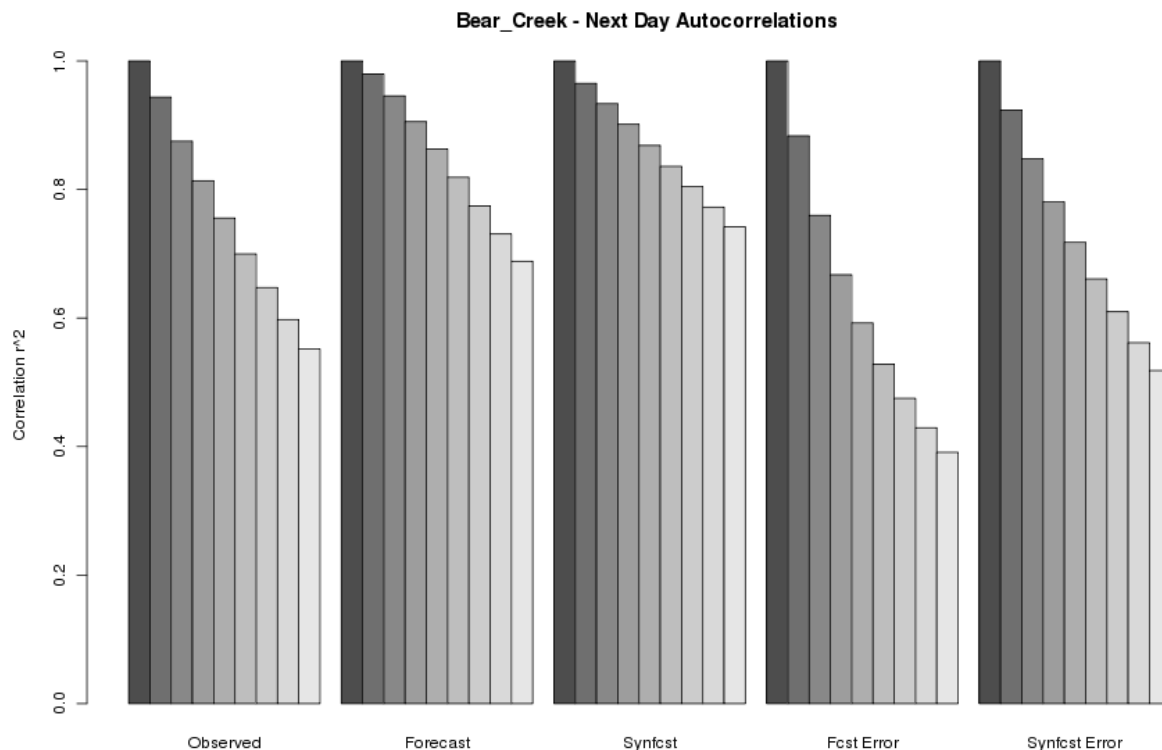
Figure 15. Autocorrelation of observed, actual forecasted and synthetic forecasted wind power at the Bear Creek generation facility. Each bar represents a time shift of one hour from the previous bar. The first bar on the left represents a time shift of zero; therefore, the correlation is perfect.

The correlation of forecast errors as a function of distance between projects was evaluated next. The correct modeling of the spatial correlation of forecast errors was an important consideration for this study as it affects the aggregate impact of many wind projects over a large region. If the synthesized forecast errors are not correlated enough between projects, then the aggregate forecast error will be underestimated, and therefore also the impacts of those errors on system operations; overestimating the degree of correlation between projects will have the opposite effect. The actual and synthetic forecasts were correlated with the observed power output for each plant and plotted versus the distance between them (Figure 16 and Figure 17). This gives an indication of how the forecasts, power, and the errors between them correlate in space. Although the synthetic forecasts are less correlated at nearby facilities, it was found that the errors correlate very similarly.
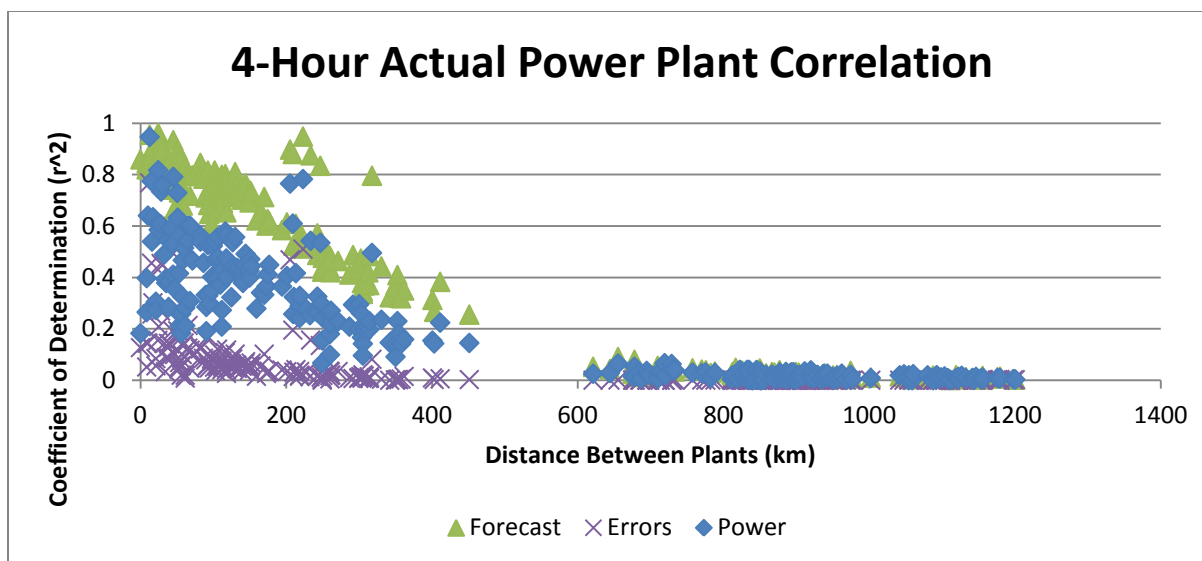
Figure 16. Forecast correlation as a function of distance between projects with a 4-hour forecast horizon. Shown for the actual forecast, observed power, and the error between them.
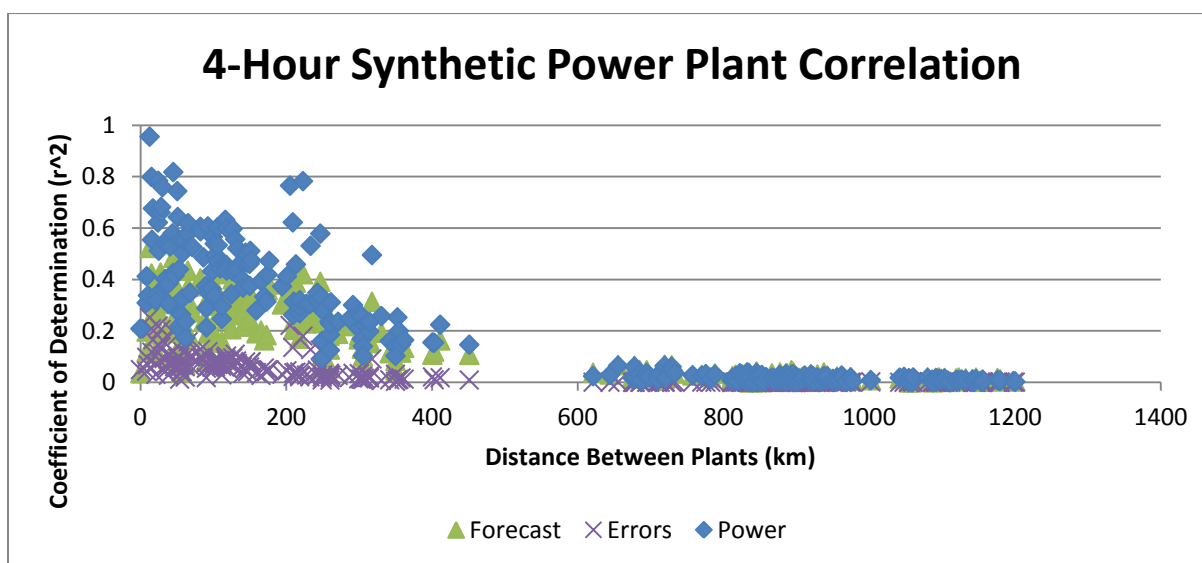
Figure 17. Same as Figure 16, but for the synthetic forecast.

The aggregation of forecast errors is considered to be the most important piece of the forecast analysis. The individual errors from each wind generation facility contribute to a system-wide error. It was found that the actual aggregated forecast errors for the next-day time horizon tend to vary from 60 and 80 GWh. As the forecast horizon increases, the variance of forecast errors increases with little change in the mean error. The distribution of errors is shown in Figure 18 for the actual forecasts and in Figure 19 for the synthetic forecasts. The plots show that there is almost no difference when comparing forecast errors on the system wide scale, with only a slight bias in the mean.
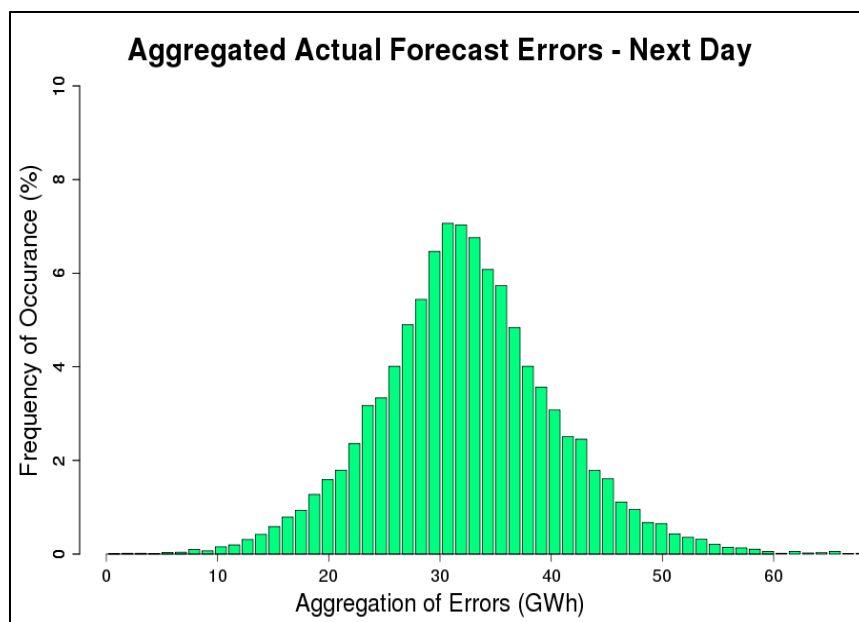
Figure 18. Distribution of aggregated actual forecasted errors for the 18 power plants for the next-day forecast. The x-axis shows the sum of forecast errors in GWh, while the y-axis shows the frequency of occurrence in %.
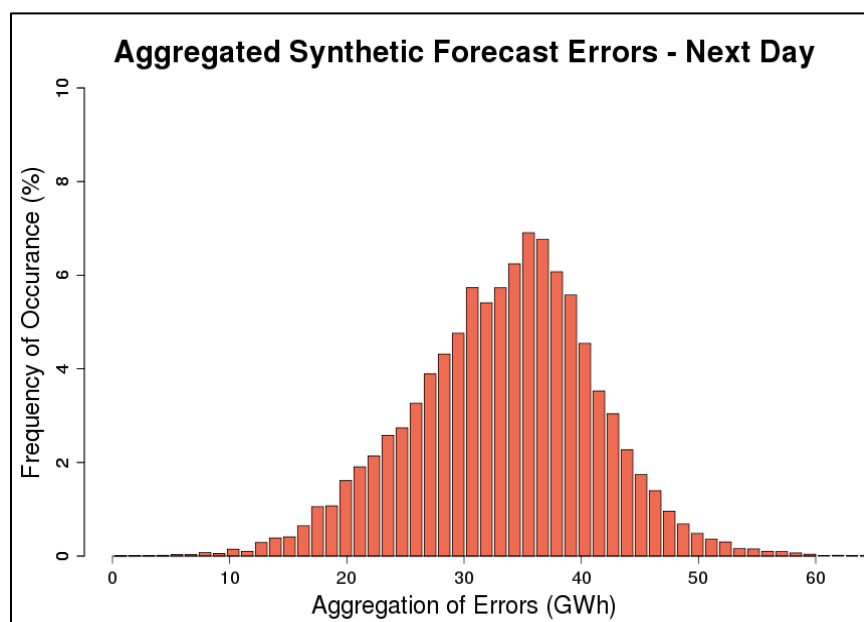
Figure 19. The same as in Figure 18, but for the synthetic forecast errors.

6.2. SOLAR

As the PV profiles depend on the modeled irradiances, it is important to capture the mean patterns and fluctuations of these variables. Irradiance measurements from six measurement stations within the PJM region were used to validate the modeled irradiances and estimate errors. Each of the monitoring stations reported measurements of GHI, DNI, and DHI, with the exception of station six, which reported

only GHI. All of the observations used for this analysis contained data from the concurrent modeling period.

The modeled GHI compares quite well with the measurement stations, with an average error of -0.01% across all of the stations for the three year period. In addition to the overall station average, several other parameters were considered for validation. The monthly and diurnal GHI profiles were computed for each station (Figure 20, Panels 1 and 2). The modeled data captures the observed seasonal and daily means very well, except for a small under-prediction of the peak midday irradiance. The modeled data was also correlated with the hourly observed data for the three year period (Figure 20 Panel 3). The agreement between the datasets was found to be acceptable, with an overall coefficient of determination of 0.731. Lastly, the step-change distribution was computed from the 60-minute averaged of irradiance (Figure 20 Panel 4). There are large step-changes for every station, which are the result of clouds passing over the measurement station. The modeled data are slightly more variable than the observed, particularly for very large changes in irradiance. Although the distributions do not match perfectly, the agreement was deemed acceptable.

The same comparisons were also carried out for the other two components of irradiance, DNI and DHI. It was found that the model consistently under-predicts the diffuse component. This was attributed to problems in the simulation of clouds. Despite this bias, the model accurately predicts the time variance of these variables, as the ramp distributions closely approximated those of observed values. Since GHI is the most important factor in the power conversion process, the validation results were deemed acceptable for this study.
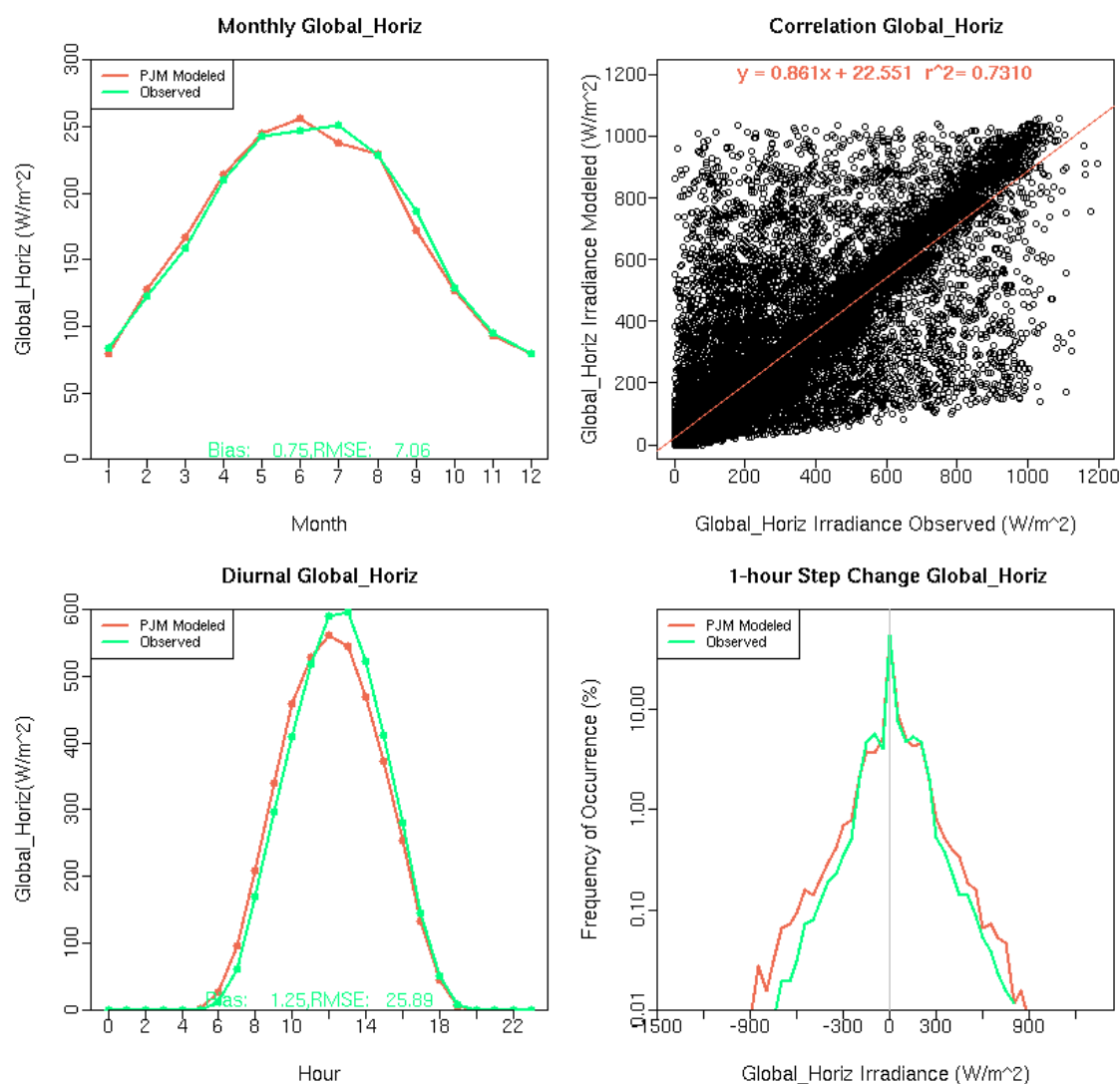
Figure 20. Comparison of modeled versus observed GHI at monitoring station in Sterling, VA. Reading down then across, panel 1 shows the average month GHI for modeled (red) and observed (green); panel 2 is the same as 1 except for it is the diurnal profile; panel 3 shows the modeled v. observed scatter plot with the best file regression line and coefficient of determination in red; panel 4 is the 1-hour step change of irradiance.

6.2.1. Power Generation

Since there was no operational solar plant output data available at the time of the study, no direct comparisons were made with actual power output. In a previous study, AWST ran the energy modeling software PVSYST[6] at one rooftop and one ground-mounted site, and the mean, maximum, and minimum gross and net power output were within 1% of values produced by the AWST power conversion method.

---

[6]A. Mermoud, "PVsyst: Software for the Study and Simulation of Photovoltaic Systems", ISE, University of Geneva www.pvsyst.com

Since the power conversion method is quite similar to the method used in PVSYST, these results should be representative of multiple locations within the PJM region.

6.2.2. Forecasts

To verify the accuracy of the synthetic solar forecast, AWST compared synthesized forecasts with the actual forecasts for the six measurement stations. It was found that the correlation of observed irradiance to synthetically forecasted irradiance (r^2=0.883) was very close to that for actual forecasts (r^2=0.902) for all stations. The synthetic forecast had a combined RMSE of 10.17% of the average GHI for all stations, where as the actual had an RMSE of 9.37%. These statistics are summarized in Table 13.

Table 13. Next day solar forecast correlation, RMSE, and MAE.

	Correlation (R)		RMS Forecast Error (%)		MA Forecast Error (%)	
Power Plant	PJM	SynFcst	PJM	Synfcst	PJM	Synfcst
Bluefield State, WV	0.888	0.848	0.098	0.114	0.05	0.054
Bondville, IL	0.91	0.895	0.093	0.101	0.046	0.048
Elizabeth City, NC	0.917	0.906	0.088	0.094	0.043	0.047
Oak Ridge, TN	0.89	0.874	0.094	0.107	0.05	0.052
Penn State Univ, PA	0.893	0.875	0.097	0.099	0.048	0.05
Sterling, VA	0.911	0.902	0.092	0.095	0.046	0.048

The autocorrelation of solar irradiance was computed for the forecasts and forecast errors, and was compared to that of the actual forecast and forecast errors. The correlation of measured to forecasted irradiance for the synthetic forecast is very similar to the actual forecast across all time shift hours (Table 14). The table and corresponding plot (Figure 21) also show that the irradiance tends to become negatively correlated for time shifts longer than 6 hours. This is a consequence of the solar cycle. The correlation of forecasts and forecast errors as a function of distance between stations was also considered for the synthesized irradiance data.The synthetic irradiance forecasts and errors exhibited a similar degree of correlation between sites as the observed irradiance forecasts.The synthetic forecasts (forecast errors) were slightly more (less) correlated than the actuals (Figure 22 and Figure 23).The greater degree of correlation between the synthetic forecast errors indicates a possible tendency to overestimate the errors when aggregated over large numbers of projects in a given region. However, the increase in correlation values is small and the functional dependence with distance is quite similar.

Table 14. Elizabeth City, NC autocorrelation of solar forecasts and forecast error reported (Pearson R Correlation).

Time Shift	Obs	PJM	Synfcst	PJM Error	Synfcst Error
0	1	1	1	1	1
1	0.891	0.936	0.904	0.501	0.480
2	0.752	0.794	0.764	0.319	0.267
3	0.563	0.600	0.582	0.202	0.135
4	0.352	0.379	0.377	0.120	0.050
5	0.143	0.156	0.169	0.066	0.007
6	-0.043	-0.047	-0.024	0.037	-0.016
7	-0.194	-0.218	-0.190	0.019	-0.024
8	-0.303	-0.347	-0.319	0.013	-0.021

ElizabethCity-NC4 Hour - Hour Autocorrelations
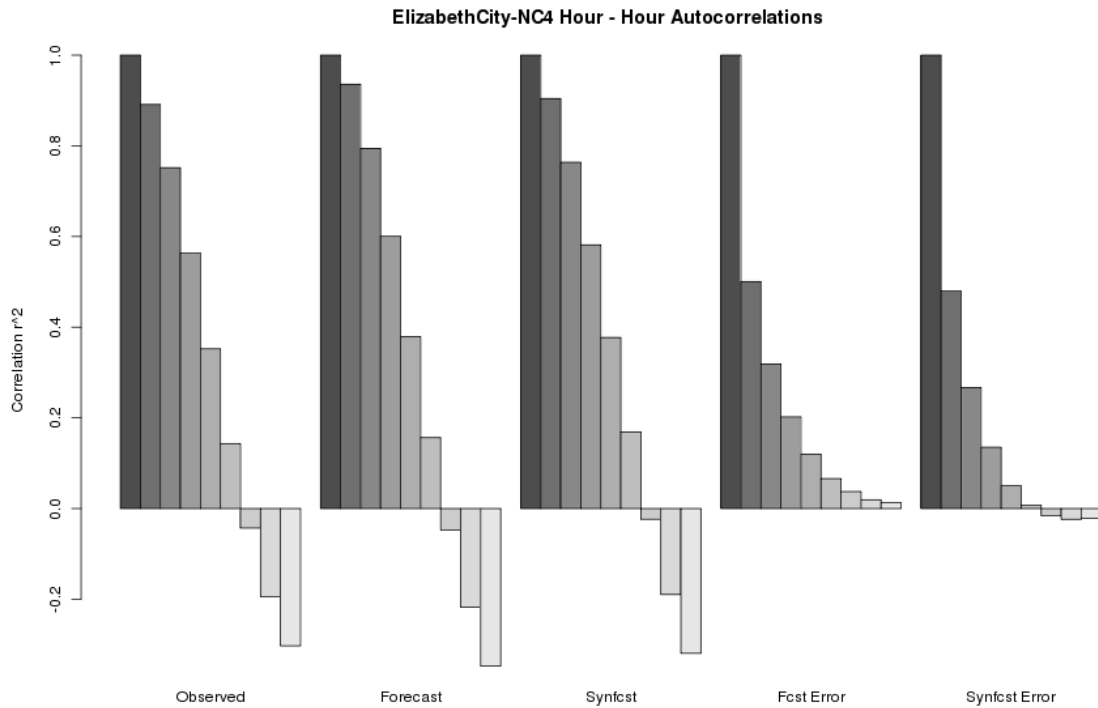
Figure 21.Autocorrelation of observed, actual forecasted and synthetic forecasted solar irradiance at the Elizabeth City, NC measurement.
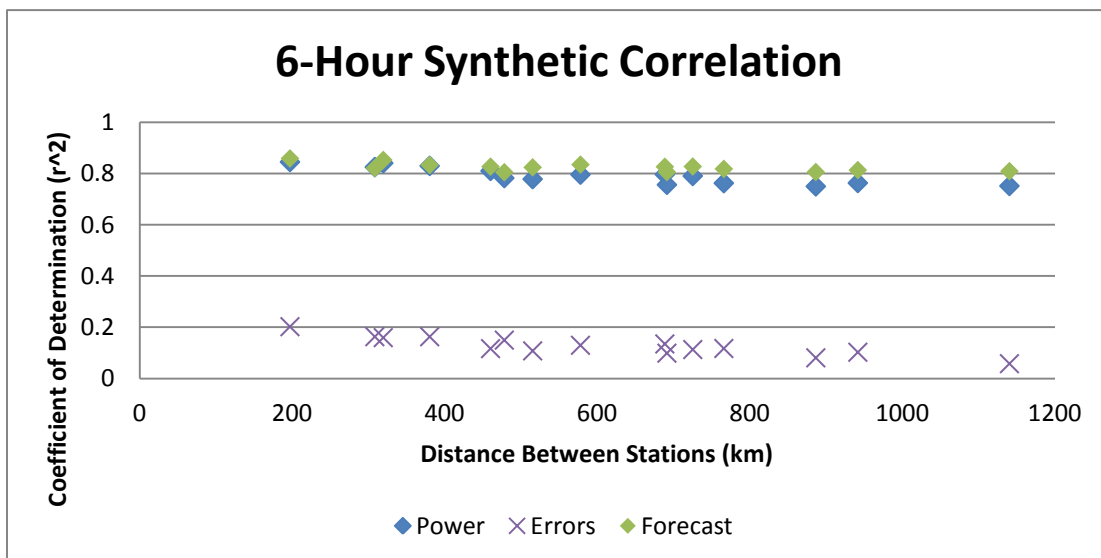
Figure 22. Forecast correlation as a function of distance between measurement stations with a 6-hour forecast horizon. Shown for the synthetic forecast, observed irradiance, and the error between them.
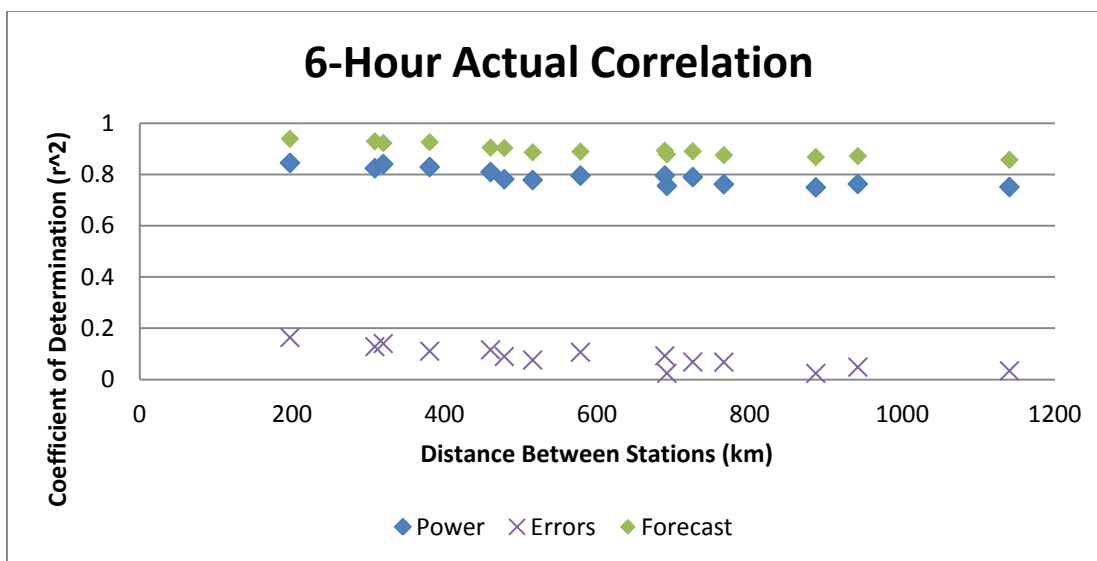
Figure 23. Same as in Figure 22, except for the actual forecasts.

7. DELIVERED DATASETS

A total of eight individual datasets were delivered by AWST for the PRIS: onshore and offshore wind power, onshore and offshore forecasts, centralized solar power, centralized solar power forecasts, distributed solar power, and distributed solar power forecasts. Each of these datasets was uploaded as compressed (zip) file to the AWS Truepower hosted ftp site.

For wind, the following data were provided in each profile:

Header: Site number, Rated capacity, Chosen IEC class, Losses (%) IEC1 IEC2 IEC3 Chosen
       Latitude Longitude
1. Date (YYYYMMDD)
2. Time (HHMM,GMT)
3. Wind speed 80m above ground surface (m/s)
4. Wind speed 100 m above ground surface (m/s)
5. Wind turbine output for the IEC class 1 power curve (MW)
6. Wind turbine output for the IEC class 2 power curve (MW)
7. Wind turbine output for the IEC class 3 power curve (MW)
8. Wind turbine output for the selected IEC power curve (MW)

For solar, the following data were provided in each profile:

9. Date (YYYYMMDD)
10. Time (HHMM,GMT)
11. Global Horizontal Irradiance (W/m^2)
12. Direct Normal Irradiance (W/m^2)
13. Diffuse Horizontal Irradiance (W/m^2)
14. Temperature 2m above ground surface (°C)
15. Wind speed 10m above ground surface (m/s)
16. Rainfall (mm)

17. Gross power output – fixed system (MW$_{DC}$)
18. Net power output – fixed system (MW$_{AC}$)
19. Gross power output – tracking system (MW$_{DC}$)
20. Net power output – tracking system (MW$_{AC}$)

Gross power output is given in MW$_{DC}$ as a function of irradiance on the plane-of-array and module characteristics. Temperature effects on the module were not considered at this point. Net power output is given in MW$_{AC}$ and represents power after losses that would be injected into the electrical grid. The net power does not include losses due to mismatched inverter sizes or electrical losses that would be expected in an operational system. In addition to the solar profiles, a site list containing the ID number, location, and plant size for each site. Two power values were provided for each site configuration in order to demonstrate how losses act on the modules.

8. SUMMARY

AWST used the three year meteorological data from the EWITS to produce power output profiles for both wind and solar renewable energy generation facilities. A site selection process was completed for onshore and offshore wind as well as for the centralized and distributed solar sites within the PJM region. The selection was designed to select representative sites that could be installed to meet and exceed renewable portfolio standards for the PJM Interconnection. Using the meteorological data, the power output profiles were developed for each of the hypothetical and planned sites using specifications from the most current power conversion technologies as of July 2011. All of the wind and solar power profiles were validated against surface measurements and were found to be acceptable for use in the PRIS.

Power and energy output were also validated with limited publicly-available generation data and industry-standard software output. Although no model is a perfect reflection of reality, results confirmed that the data represent in a realistic way the averages, seasonal and diurnal patterns, ramping behavior, and power output for wind and solar plants in the PJM region. These data sets are suitable for use in system planning and operating studies.